Article

Cell Host & Microbe

Cell Surface Proteomic Map of HIV Infection Reveals Antagonism of Amino Acid Metabolism by Vpu and Nef

Graphical Abstract

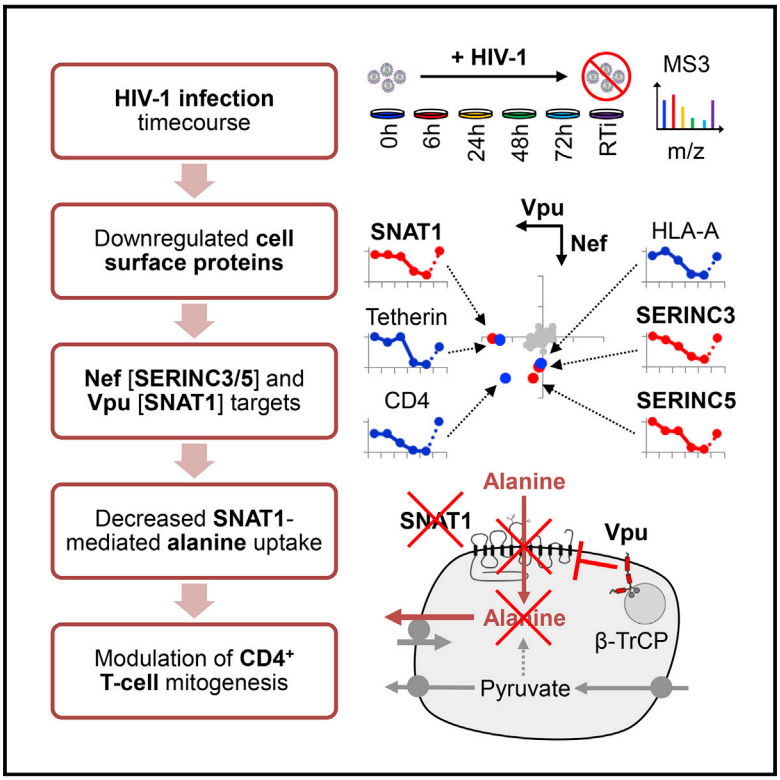

Authors

Nicholas J. Matheson, Jonathan Sumner, Kim Wals, ..., Clary B. Clish, Stuart J.D. Neil, Paul J. Lehner

Correspondence

njm25@cam.ac.uk (N.J.M.), pjl30@cam.ac.uk (P.J.L.)

In Brief

Viruses manipulate host factors to enhance their replication. Matheson et al. use functional proteomics to analyze plasma membrane proteins downregulated during HIV-1 infection. Serine carriers SERINC3/5 and alanine transporter SNAT1 were identified as Nef and Vpu targets, respectively. Antagonism of SNAT1-mediated alanine transport enables viral interference with T cell immunometabolism

Highlights

- Unbiased global analysis of T cell surface proteome remodeling during HIV infection
- >100 proteins downregulated, including Nef targets SERINC3/5 and Vpu target SNAT1
- β-TrCP-dependent SNAT1 downregulation acquired by pandemic SIVcpz/HIV-1 viruses
- Uptake of exogenous alanine by SNAT1 critical for primary CD4+ T cell mitogenesis

Matheson et al., 2015, Cell Host & Microbe *18*, 409–423
October 14, 2015
http://dx.doi.org/10.1016/j.chom.2015.09.003

Cell Host & Microbe
Article

Cell Surface Proteomic Map of HIV Infection Reveals Antagonism of Amino Acid Metabolism by Vpu and Nef

Nicholas J. Matheson,[1,*] Jonathan Sumner,[2] Kim Wals,[1] Radu Rapiteanu,[1] Michael P. Weekes,[1] Raphael Vigan,[2] Julia Weinelt,[2] Michael Schindler,[3,4] Robin Antrobus,[1] Ana S.H. Costa,[5] Christian Frezza,[5] Clary B. Clish,[6] Stuart J.D. Neil,[2] and Paul J. Lehner[1,*]

[1]Cambridge Institute for Medical Research, University of Cambridge, Cambridge Biomedical Campus, Cambridge CB2 0XY, UK
[2]Department of Infectious Diseases, King's College London School of Medicine, Guy's Hospital, London SE1 9RT, UK
[3]Helmholtz Center Munich, Institute of Virology, 85764 Neuherberg, Germany
[4]Institute of Medical Virology and Epidemiology of Viral Diseases, University Clinic Tübingen, 72076 Tübingen, Germany
[5]MRC Cancer Unit, Hutchison/MRC Research Centre, University of Cambridge, Cambridge Biomedical Campus, Cambridge CB2 0XZ, UK
[6]The Broad Institute of the Massachusetts Institute of Technology and Harvard, Cambridge, MA 02142, USA
*Correspondence: njm25@cam.ac.uk (N.J.M.), pjl30@cam.ac.uk (P.J.L.)
http://dx.doi.org/10.1016/j.chom.2015.09.003

SUMMARY

Critical cell surface immunoreceptors downregulated during HIV infection have previously been identified using non-systematic, candidate approaches. To gain a comprehensive, unbiased overview of how HIV infection remodels the T cell surface, we took a distinct, systems-level, quantitative proteomic approach. >100 plasma membrane proteins, many without characterized immune functions, were downregulated during HIV infection. Host factors targeted by the viral accessory proteins Vpu or Nef included the amino acid transporter SNAT1 and the serine carriers SERINC3/5. We focused on SNAT1, a β-TrCP-dependent Vpu substrate. SNAT1 antagonism was acquired by Vpu variants from the lineage of SIVcpz/HIV-1 viruses responsible for pandemic AIDS. We found marked SNAT1 induction in activated primary human CD4+ T cells, and used Consumption and Release (CoRe) metabolomics to identify alanine as an endogenous SNAT1 substrate required for T cell mitogenesis. Downregulation of SNAT1 therefore defines a unique paradigm of HIV interference with immunometabolism.

INTRODUCTION

HIV-1 viruses of the AIDS pandemic encode four "accessory proteins" (Vif, Vpr, Vpu, and Nef) dispensable for viral replication in vitro, but essential for viral pathogenesis in vivo (Malim and Emerman, 2008). Vpu and Nef are multifunctional adaptors that downregulate cell surface proteins to counteract host-cell restriction and evade the immune response (Haller et al., 2014; Tokarev and Guatelli, 2011). Targets have typically been identified using non-systematic, candidate approaches and include the HIV receptor CD4, the restriction factor tetherin, and the MHC I molecules HLA-A/B (Tokarev and Guatelli, 2011).

Among primate lentiviruses, a correlation is observed between viral pathogenicity and expression of Vpu, with CD4+ T cell decline and progression to AIDS markedly faster in HIV-1 than HIV-2, and increased mortality in chimpanzees infected with SIVcpz (Keele et al., 2009). Vpu induces substrate-specific ubiquitination of CD4 and tetherin through recruitment of the SCF-β-TrCP E3 ligase complex via a constitutively phosphorylated phosphodegron in its cytoplasmic tail (Douglas et al., 2009; Margottin et al., 1998; Mitchell et al., 2009). In the SIV-HIV (SHIV) macaque model of HIV, CD4+ T cell loss is abrogated by deletion of Vpu, scrambling of its transmembrane domain, or mutation of its β-TrCP-binding phosphodegron (Hout et al., 2005; Singh et al., 2003; Stephens et al., 2002). This effect is unlikely to be attributable to loss of Vpu-mediated downregulation of macaque CD4 or tetherin because CD4 is also efficiently downregulated by Nef, and pig-tailed macaque tetherin is antagonized by SIVmac Nef, but not by HIV-1 Vpu (Zhang et al., 2009). Together, these data point to the existence of additional, biologically important, β-TrCP-dependent Vpu substrates.

In this study, we combine plasma membrane enrichment through selective aminooxy-biotinylation (Plasma Membrane Profiling; PMP) with Tandem Mass Tag (TMT) and Stable Isotope Labeling by Amino Acids in Cell Culture (SILAC)-based quantitative proteomics to describe global changes in the cell surface landscape of an HIV-infected T cell, including expression time courses of >800 plasma membrane proteins (Weekes et al., 2013, 2014). Our unbiased, comprehensive analysis reveals downregulation of >100 HIV-1 targets, particularly proteins involved in cell adhesion, leukocyte activation, and transmembrane transport, and is presented as a searchable database to facilitate data mining.

In addition to their known substrates, we show that Vpu is necessary and sufficient for β-TrCP-dependent degradation of the amino acid transporter SNAT1, and Nef is sufficient for downregulation of the serine carriers SERINC3 and SERINC5. We apply an unbiased, CoRe metabolomic approach to identify the non-essential amino acid alanine as an endogenous SNAT1

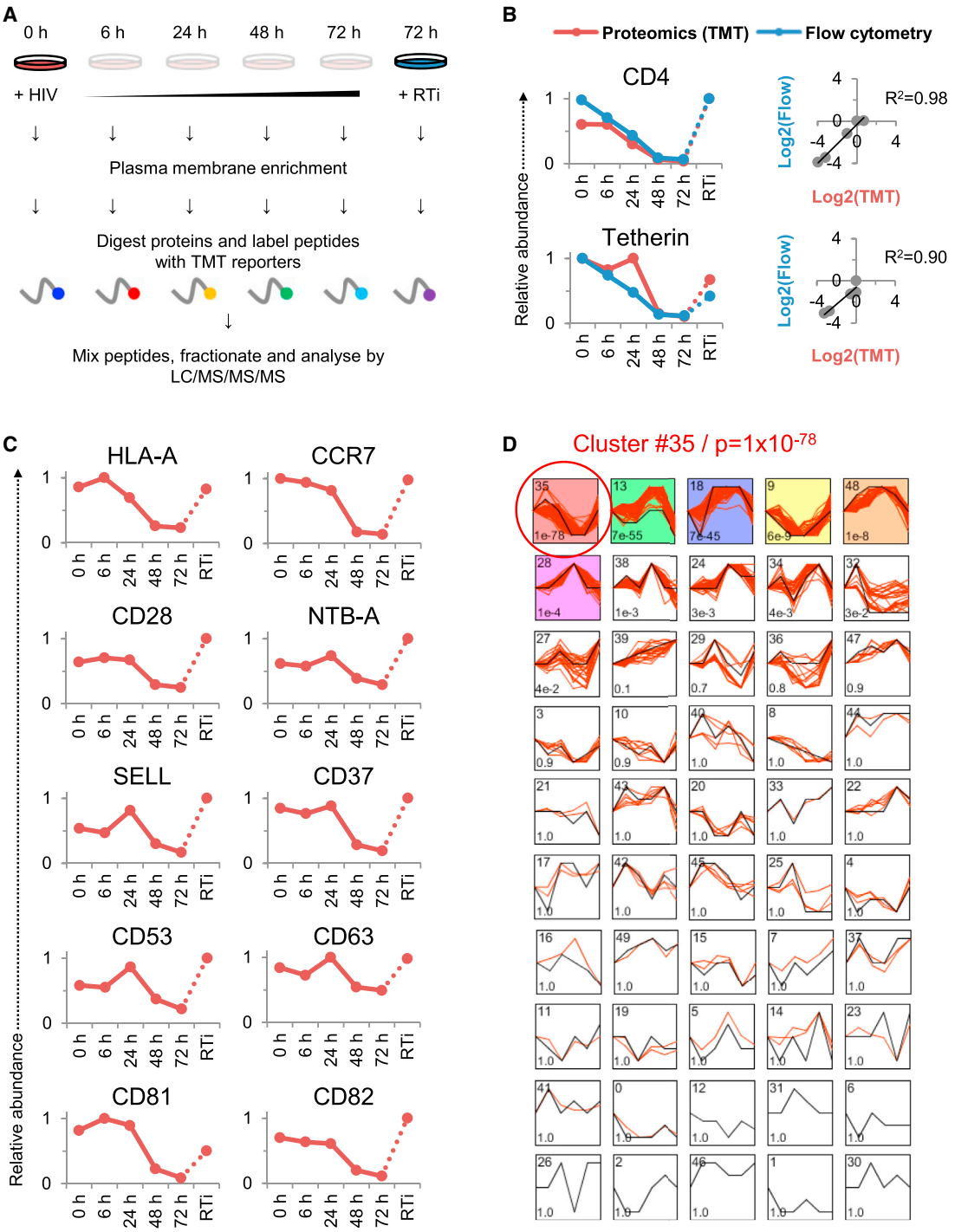

Figure 1. TMT-Based Proteomic Time Course of Plasma Membrane Protein Expression in HIV-1-Infected Cells

(A) Workflow of TMT-based 6-plex PMP time course experiment. In subsequent figures, time points 1–5 show plasma membrane protein expression 0, 6, 24, 48, and 72 hr after HIV-1 infection (where 0 hr = uninfected cells), and time point 6 shows plasma membrane protein expression 72 hr after HIV-1 infection in the presence of reverse transcriptase inhibitors (RTi). NL4-3-deltaE-EGFP HIV-1 viruses at an MOI of 10 were used for all proteomic experiments.

(B) Comparison of temporal profiles of CD4 and tetherin obtained by proteomic (TMT) versus flow cytometric quantitation. Cells from (A) were stained with anti-CD4 and anti-tetherin antibodies at the indicated time points and analyzed by flow cytometry. Relative abundance is expressed as a fraction of maximum TMT reporter ion or fluorescence intensity. For linear regression, log2(fold change compared with uninfected cells) is shown.

(C) Temporal profiles of previously reported targets for HIV-mediated downregulation.

(legend continued on next page)

substrate in primary human CD4+ T cells, and show that extracellular alanine is critical for T cell mitogenesis. Restricting alanine uptake through Vpu-mediated downregulation of SNAT1 therefore represents a viral strategy to regulate immune cell activation.

RESULTS

Systematic Time Course Analysis of T Cell Surface Protein Expression during HIV-1 Infection

To gain a comprehensive, unbiased overview of plasma membrane protein regulation by HIV-1, we used PMP to measure expression levels of cell surface proteins in CEM-T4 T cells infected with HIV-1 (Figure 1A) (Weekes et al., 2013, 2014). By spinoculating cells with Env-deficient, VSVg-pseudotyped virus, we ensured a synchronous, single-round infection, and by using a multiplicity of infection (MOI) sufficient to infect >90% of cells, we minimized confounding effects from bystander (uninfected) cells (Figure S1A). We exploited 6-plex TMT quantitation to compare plasma membrane protein abundance in uninfected cells (0 hr), at 4 time points following HIV-1 infection (6, 24, 48, and 72 hr) and, to control for cellular changes occurring in the absence of de novo viral gene expression, in cells infected for 72 hr in the presence of reverse transcriptase inhibitors (RTi). In total, 2,320 proteins were quantitated, including 804 proteins previously reported to localize to the plasma membrane (Figure S1B). The complete dataset is shown in interactive Table S1, which allows generation of temporal profiles for any quantitated genes of interest.

We observed a strong correlation between expression time courses determined by mass spectrometry and flow cytometry for CD4 (R^2 = 0.98) and tetherin (R^2 = 0.90) (Figure 1B), saw marked time-dependent depletion of cell surface HLA-A, and confirmed progressive downregulation of other known HIV-1 targets (CCR7, CD28, NTB-A, SELL, and the tetraspanins CD37/53/63/81/82) (Figure 1C) (Haller et al., 2014; Lambelé et al., 2015; Ramirez et al., 2014; Shah et al., 2010; Swigut et al., 2001; Vassena et al., 2015). Downregulation of CD71 and the chemokine receptors is controversial, with our data suggesting depletion of cell surface CD71, CXCR4, and CCR5 (Figure S1C). As expected, VSVg levels increased immediately after infection, then rapidly declined (Figure S1D).

Discovery of Cell Surface Targets Depleted by HIV-1

To identify host factors regulated by HIV-1 without observer bias based on known biological function, we used the Short Time Series Expression Miner (STEM) to cluster proteins according to patterns of temporal expression and identify profiles occurring more frequently than expected by chance (Figure 1D). The most enriched profile comprised 134 proteins showing progressive time-dependent downregulation, abolished by reverse transcriptase inhibitors (Cluster #35; $p = 10^{-78}$). Proteins in this cluster, which include CD4, tetherin, and HLA-A, represent candidate HIV-1 cell surface targets (Table S2).

We validated these candidates in an independent infection time course experiment using SILAC as an alternative quantitative proteomic approach (Figures 2A and 2B) and confirmed downregulation of a functionally and structurally diverse set of proteins with available antibody reagents (CD43/47/162 and NOTCH1) by flow cytometry in CEM-T4s and primary human CD4+ T cells infected with HIV-1 (Figure S2A).

Functional Analysis of Progressively Downregulated HIV-1 Targets

To identify biological functions targeted by HIV-1 in an unbiased fashion, we used the Database for Annotation, Visualization and Integrated Discovery (DAVID) to determine gene ontology "molecular function" and "biological process" annotations over-represented in Cluster #35 compared with other quantitated proteins. The cluster was enriched for terms relating to cell adhesion, leukocyte activation, and transmembrane transport. These categories intersect processes known to be modulated by HIV-1 and provide a framework for interpreting both previously identified and novel HIV-1 targets. We therefore mined our data for downregulated proteins with closely related functions (Figures 2C–2F and Table S3).

Cell adhesion molecules regulate leukocyte trafficking and NK cell killing. Modulation of lymphocyte migration through targeting of SELL and CCR7 (Figure 1C) is proposed to facilitate HIV-1 immune avoidance (Ramirez et al., 2014; Vassena et al., 2015), and downregulation of NTB-A (Figure 1C) protects HIV-infected cells from NK cell lysis (Shah et al., 2010). We now show that HIV-1 also downregulates NCR3LG1 (B7H6; Figure 2D), a ligand for the NK activating receptor NKp30 found on activated monocytic cells in vivo (Brandt et al., 2009; Matta et al., 2013). Flow cytometry confirmed reduced Ig-NKp30 binding to HIV-1-infected CEM-T4 cells (Figure S2B).

HIV-1 replication is critically dependent on the activation state of infected cells, and the virus employs multiple strategies to modulate T cell activation and maximize replication in vivo (Abraham and Fackler, 2012). Attention has focused on downregulation of CD3 by Nef variants of non-pathogenic SIVs, attenuated in HIV-1 Nef (Schindler et al., 2006). Conversely, our data revealed downregulation of numerous other immunoreceptors with important functions in T cell activation (Figure 2E), along with a range of transmembrane transporters with no known roles in the immune system, particularly amino acid transporters (Figure 2F). Since T cell activation requires profound upregulation in amino acid metabolism (Wang et al., 2011), we predict that these proteins have important, but unrecognized, functions in T cell biology.

Systematic Plasma Membrane Proteomic Analysis of HIV-1 Accessory Proteins Vpu and Nef

Depletion of most known HIV-1 cell surface targets has been attributed to Vpu and/or Nef (Haller et al., 2014; Tokarev and Guatelli, 2011). To assign downregulation of proteins in Cluster #35 to particular viral genes, we applied an unbiased,

(D) Identification of enriched temporal profiles by STEM. Model temporal profiles (black) and matched experimental protein expression profiles (red) are shown. Each box includes a profile identification number (top left) and an unadjusted p value (bottom left). Colored boxes indicate model profiles assigned more proteins than expected by chance alone (Bonferroni-adjusted p values < 0.05).
See also Figure S1 and Tables S1 and S2.

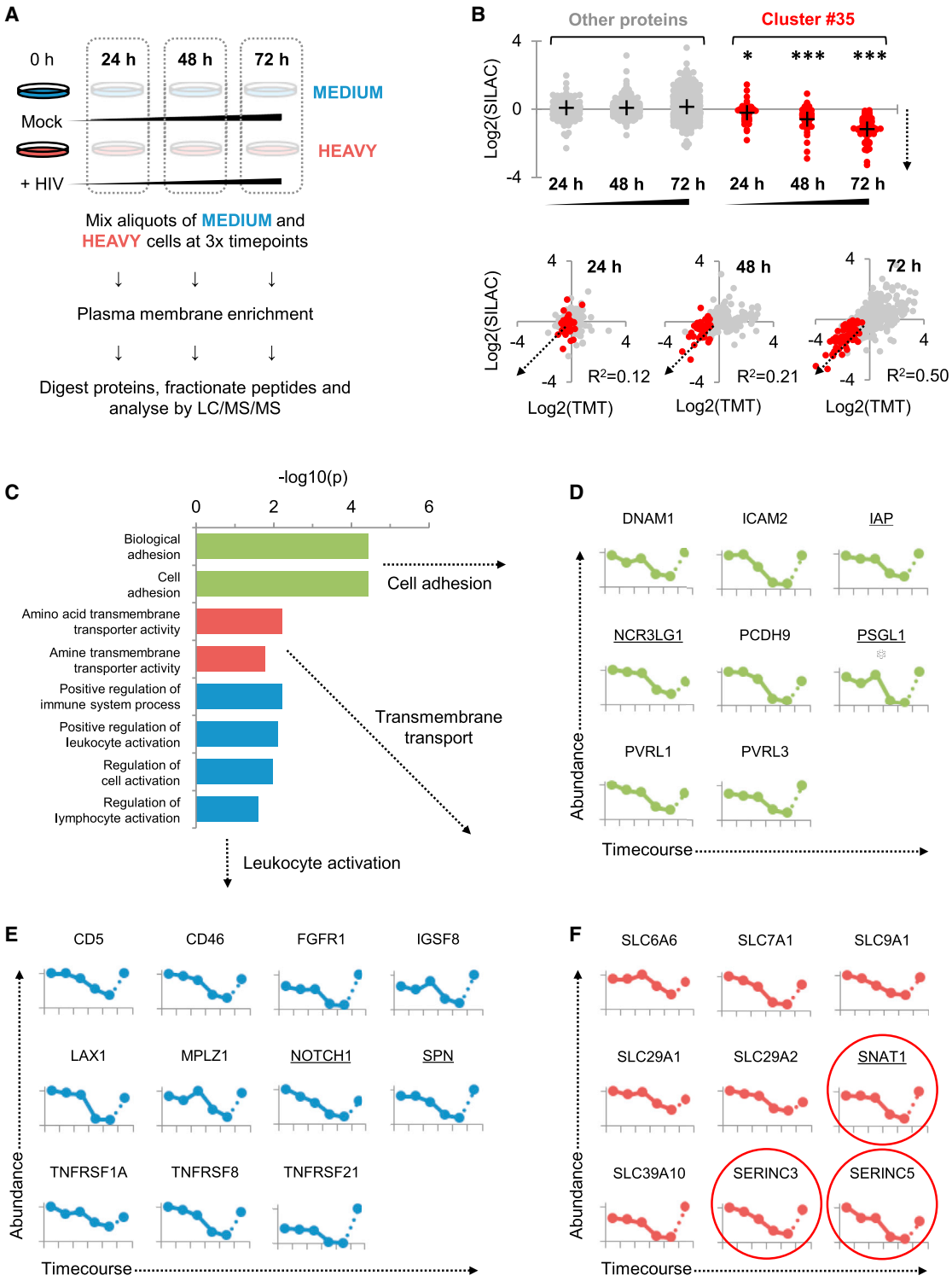

Figure 2. SILAC-Based Proteomic Validation and Functional Analysis of Cell Surface Targets Downregulated by HIV-1

(A) Workflow of SILAC-based 3-way PMP time course experiment.

(B) Validation of HIV-1 targets (upper panel) and comparison between SILAC- and TMT-based time course experiments (lower panel). Log2(fold change compared with mock/uninfected cells) at 24, 48, and 72 hr is shown for proteins from Cluster #35 (red) versus all other quantitated proteins (gray). Downregulation by HIV-1 is indicated by dotted arrows. Proteins identified by >1 unique peptide in both TMT and SILAC experiments are shown. Crosses indicate mean values. *$p < 0.05$; ***$p < 0.001$.

(legend continued on next page)

systematic approach to define Vpu and Nef substrates. SILAC-based PMP was used to compare expression levels of cell surface proteins in CEM-T4s infected with either Vpu- or Nef-deficient viruses (Figures 3A and S3A), or transduced with Vpu or Nef as single genes (Figures 3B and S3B). As positive controls, we found that Vpu depleted cell surface CD4 and tetherin, while Nef depleted cell surface CD4 and HLA-A (Figures 3A and 3B). Surprisingly, many HIV-1 cell surface targets were downregulated efficiently by both Vpu- and Nef-deficient viruses and not by overexpression of Vpu and Nef as single genes, suggesting Vpu- and Nef-independent mechanisms.

Targeting of Amino Acid Metabolism by Vpu and Nef

As well as their known targets, we found Vpu to be both necessary and sufficient for downregulation of the amino acid transporter SNAT1 (Figures 2F and 3A–3B), and Nef to be sufficient for downregulation of the serine carriers SERINC3 and SERINC5 (Figures 2F and 3A–3B). This effect was specific within the SERINC family, because SERINC1 was induced rather than downregulated (Figure S1E). While this manuscript was in preparation, SERINC3 and SERINC5 were independently identified as HIV-1 restriction factors using orthogonal approaches (M. Pizzato, personal communication; H. Gottlinger, personal communication). We confirmed restriction of infectious HIV-1 viral production by SERINC5, antagonized by Nef (Figure S3C). Conversely, SNAT1 does not act as an HIV-1 restriction factor (Figure S3D). Instead, we hypothesized that antagonism of SNAT1-dependent amino acid transport by Vpu may modulate T cell activation.

We confirmed Vpu-dependent depletion of endogenous SNAT1 from the plasma membrane of transduced cells by confocal and total internal reflection (TIRF) microscopy (Figures S4A and S4B). As well as decreased expression at the cell surface, depletion of total SNAT1 was seen by immunoblot of CEM-T4s infected with WT or Nef-deficient HIV-1, but not with Vpu-deficient virus (Figures 3C, lanes 2–4, 3D, lanes 2 and 4, and S4C), and by immunoblot of CEM-T4s transduced with Vpu, but not Nef (Figure 3E, lane 5).

Previous studies have suggested that SNAT1 is predominantly expressed in the CNS (Gu et al., 2001; Varoqui et al., 2000). We found SNAT1 protein to be poorly expressed in resting primary human CD4+ T cells but dramatically induced following mitogenic T cell stimulation (Figures 3F, lanes 2–5, and 3G, panel 2). Furthermore, Vpu depletes SNAT1 from activated primary human CD4+ T cells both in the context of viral infection (Figures S4D and S4E) and as a single gene in transduced cells purified by Antibody-Free Magnetic Cell Sorting (AFMACS; Figures 3G, panel 5, 3H, lane 5, and S4F) (Matheson et al., 2014).

Ubiquitination and β-TrCP-Dependent Endolysosomal Degradation of SNAT1

To probe the mechanism of Vpu-mediated SNAT1 depletion, we confirmed that Vpu binds endogenous SNAT1 (Figure 4A, lanes 2 and 4) and leads to SNAT1 ubiquitination (Figure 4B, lane 5). As with CD4 and tetherin, downregulation of SNAT1 is rescued by mutation of the Vpu phosphodegron responsible for β-TrCP recruitment (S52, 56A) (Figures 3G, panel 6, 3H, lane 6, 4F, and S5A) and by RNAi-mediated depletion of β-TrCP (Figure 4C, lane 3).

Vpu mediates degradation of CD4 by hijacking the endoplasmic reticulum-associated degradation (ERAD) pathway (Margottin et al., 1998; Schubert et al., 1998) and antagonizes tetherin by co-opting the endolysosomal degradative pathway (Douglas et al., 2009; Mitchell et al., 2009). SNAT1 degradation is rescued by incubation with vacuolar ATPase inhibitors, but not proteasome inhibitors (Figure 4D, lanes 5 and 6), and by RNAi-mediated depletion of TSG101 (Figure 4E, lane 3), suggesting that, as for tetherin, SNAT1 is degraded in endolysosomes by the ESCRT machinery.

Downregulation of tetherin is abolished by substitution of conserved amino acid residues W22 or A14 in the transmembrane domain of Vpu, and W22 is also critical for downregulation of CD4 (Vigan and Neil, 2010). While the W22A mutation abolished downregulation of all 3 Vpu substrates, SNAT1 and CD4 downregulation were preserved in the presence of the A14L mutation (Figure 4F, lane 4, and Figure S4A). The same pattern of SNAT1 downregulation was observed with equivalent mutations in a patient-derived Vpu (Figure S5B) and with Vpu mutants in the context of viral infection (Figure S5C). The pathway for SNAT1 degradation by Vpu therefore shares the cellular machinery used for antagonism of tetherin but occurs independently of tetherin downregulation and may be dissociated from it by the A14L mutation.

CoRe Metabolomic Analysis of SNAT1-Depleted Primary Human CD4+ T Cells

When overexpressed in vitro, SNAT1 mediates uptake of a range of small neutral amino acids (Gu et al., 2001; Varoqui et al., 2000). Transport by SNAT1 is Na dependent and sensitive to competition by the model substrate α-methylaminoisobutyric acid (MeAIB), a specific inhibitor of amino acid transport System A (Mackenzie and Erickson, 2004). Based on its functional characteristics and pattern of expression, SNAT1 has primarily been considered a neuronal glutamine transporter (Chaudhry et al., 2002).

To identify endogenous SNAT1 substrates in primary human CD4+ T cells in an unbiased fashion, we combined an "activation-rest" strategy for shRNA knockdown (Monroe et al., 2014) with Consumption and Release (CoRe) metabolomics (Jain et al., 2012) (Figure 5A). Pure populations of transduced cells expressing control or SNAT1-specific shRNAs were generated by AFMACS (Figures 5B and S6A) (Matheson et al., 2014). After resting for 7–10 days, control and SNAT1-depleted cells were re-stimulated using CD3/CD28 Dynabeads. A marked reduction

(C) Gene ontology "molecular function" and "biological process" terms enriched among proteins from Cluster #35. DAVID functional annotation clusters with adjusted p values < 0.05 and containing terms with Bonferroni-adjusted p values < 0.05 are shown. Further details are included in Table S3.
(D–F) Temporal profiles of downregulated proteins associated with cell adhesion (D), leukocyte activation (E), and transmembrane transport (F). Proteomic quantitation and time points are as for Figures 1B–1C. Proteins exhibiting >2-fold downregulation compared with uninfected cells in both TMT and SILAC experiments are shown, and proteins subsequently validated using flow cytometry or immunoblot are underlined.
See also Figure S2 and Table S2.

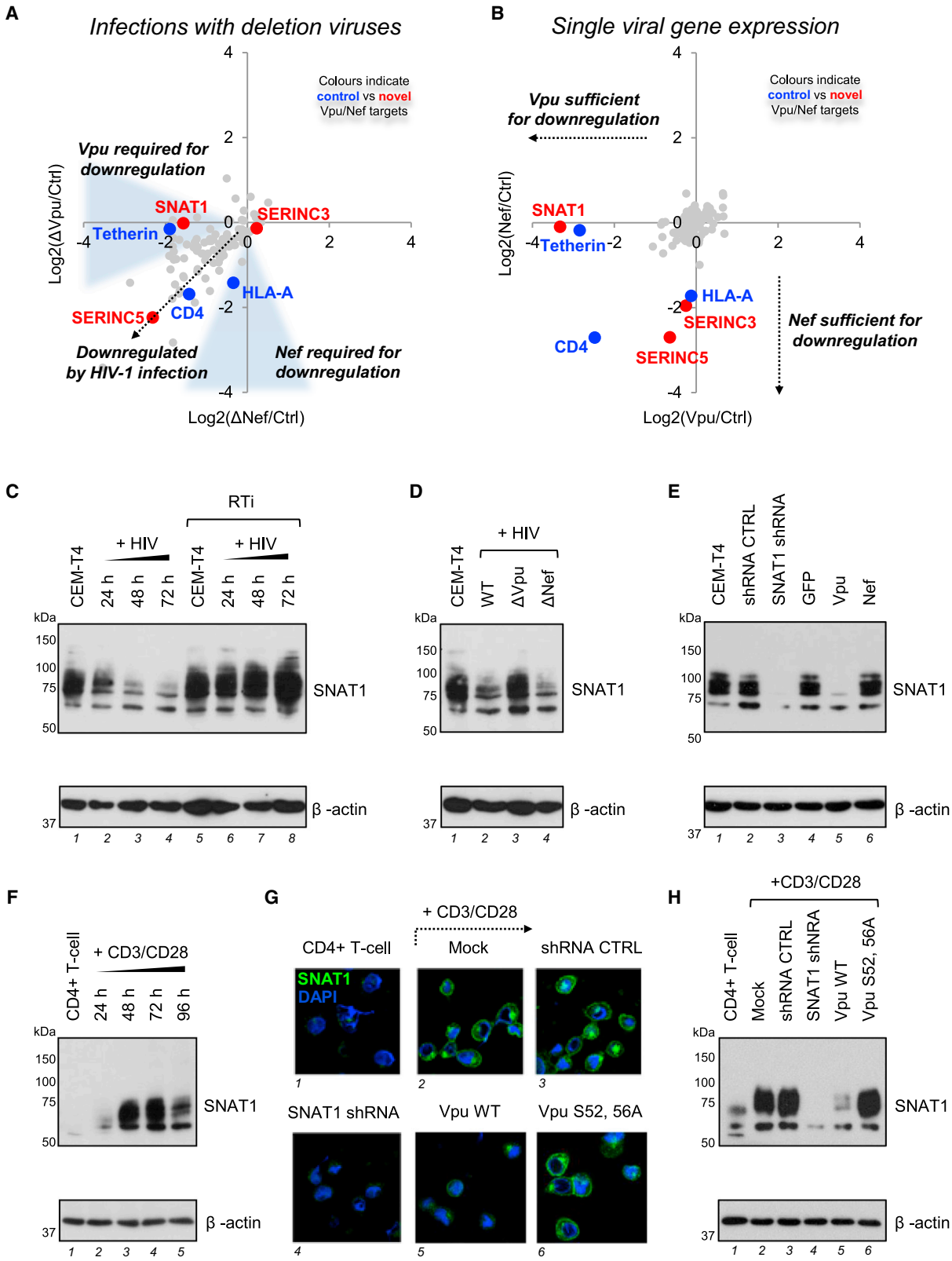

Figure 3. Proteomic Analysis of Vpu and Nef Targets and Identification of SNAT1 as a Vpu Substrate

(A and B) SILAC-based quantitation of plasma membrane proteins in cells infected with Vpu-deficient (y axis) versus Nef-deficient (x axis) HIV-1 viruses (A) and cells transduced with Vpu (x axis) versus Nef (y axis) as single genes (B). Log2(fold change compared with uninfected [A] or GFP-transduced [B] cells)

(legend continued on next page)

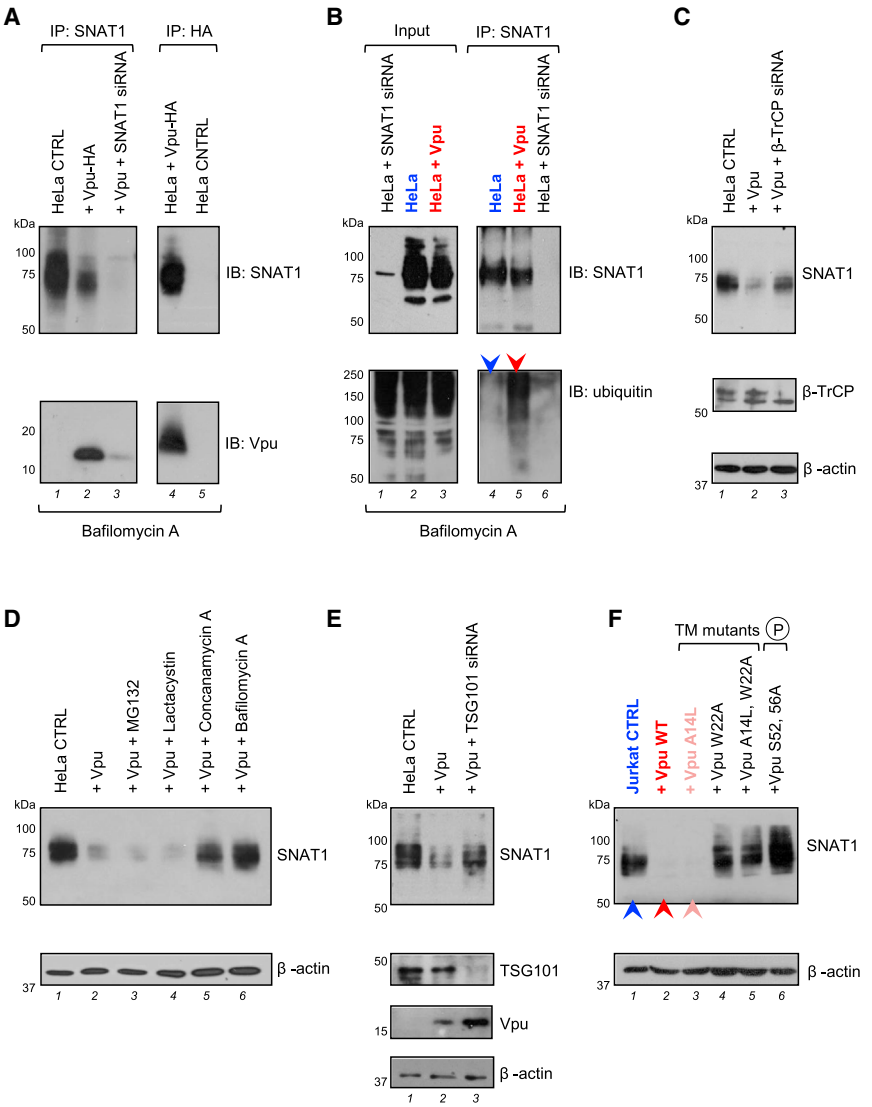

Figure 4. Mechanism of SNAT1 Depletion by Vpu

(A) Interaction of SNAT1 with Vpu. HeLa cells stably transduced with Vpu-HA were immunoprecipitated with anti-SNAT1 (G63; first panel) or anti-HA (second panel) antibodies and immunoblotted with anti-SNAT1 (H60) or anti-Vpu antibodies. Untransduced HeLas transfected with SNAT1-specific siRNA were included as controls.

(B) Ubiquitination of SNAT1 by Vpu. HeLa cells stably transduced with Vpu-HA were either immunoblotted with anti-SNAT1 (H60) and anti-ubiquitin antibodies (first panel) or immunoprecipitated with anti-SNAT1 (G63) antibody, re-immunoprecipitated with anti-SNAT1 (H60) antibody, and immunoblotted with anti-SNAT1 (H60) and anti-ubiquitin antibodies (second panel). Untransduced HeLas transfected with SNAT1-specific siRNA were included as controls. Ubiquitinated SNAT1 in control (blue arrow) and Vpu-expressing (red arrow) HeLas is highlighted.

(C) β-TrCP-dependent depletion of SNAT1. HeLa cells stably transduced with Vpu-HA were transfected with control or β-TrCP-specific siRNA then immunoblotted.

(D and E) SNAT1 depletion via an endolysosomal pathway. HeLa cells stably transduced with Vpu-HA were either treated with MG132, lactacystin, concanamycin, or bafilomycin (D) or transfected with control or TSG101-specific siRNA (E) then immunoblotted.

(F) Molecular determinants of SNAT1 down-regulation. Jurkats stably expressing Vpu WT or indicated Vpu mutants were immunoblotted. Cells transduced with empty vector (blue), Vpu WT (red), and Vpu A14L (pink) are highlighted. The same cells stained with anti-CD4 or anti-tetherin antibodies and analyzed by flow cytometry are shown in Figure S5A.

See also Figure S5.

in proliferation of SNAT1-depleted cells was observed (Figures 5C and S6A). Culture supernatants were sampled at baseline, 24, and 48 hr, and extracellular metabolite fluxes were calculated on a per-cell basis. In total, data for consumption and release of 126 metabolites, including 19 natural amino acids, were used to derive CoRe metabolomic profiles of control and SNAT1-depleted cells. Principal component analysis readily distinguished these profiles, particularly at 48 hr (Figure 5D, upper panels). Surprisingly, across all measured metabolites, the most significant difference was in net alanine release, with no difference in net glutamine consumption (Figure 5D, middle and lower panels).

is shown for proteins from Cluster #35. Figures S3A and S3B selectively enlarge the lower left quadrant of each scatterplot. Proteins identified by >1 unique peptide are shown.

(C) SNAT1 depletion by HIV-1 infection. CEM-T4s infected with WT NL4-3-deltaE-EGFP HIV-1 virus in the presence or absence of RTi were immunoblotted at the indicated time points. An MOI of 10 was used, and infection controls are shown in Figure S4C.

(D) Rescue of SNAT1 in the absence of Vpu. CEM-T4s infected with WT, Vpu-deficient, or Nef-deficient HIV-1 NL4-3-deltaE-EGFP viruses were immunoblotted at 48 hr. An MOI of 10 was used, and infection controls are shown in Figure S4C.

(E) SNAT1 depletion by Vpu. CEM-T4s stably transduced with GFP, Vpu, or Nef were immunoblotted. Untransduced CEM-T4s and CEM-T4s stably transduced with control or SNAT1-specific shRNAs were included as controls.

(F) SNAT1 induction in activated primary T cells. Primary human $CD4^+$ T cells activated with CD3/CD28 Dynabeads were immunoblotted at the indicated time points.

(G and H) SNAT1 depletion by Vpu in activated primary T cells. Primary human $CD4^+$ T cells were activated with CD3/CD28 Dynabeads and mock transduced or transduced with the indicated shRNA or Vpu constructs. After purification by AFMACS (Figure S4F), cells were either rested or re-stimulated with CD3/CD28 Dynabeads and immunoblotted (G) or analyzed by confocal microscopy (H) at 48 hr.

See also Figures S3 and S4.

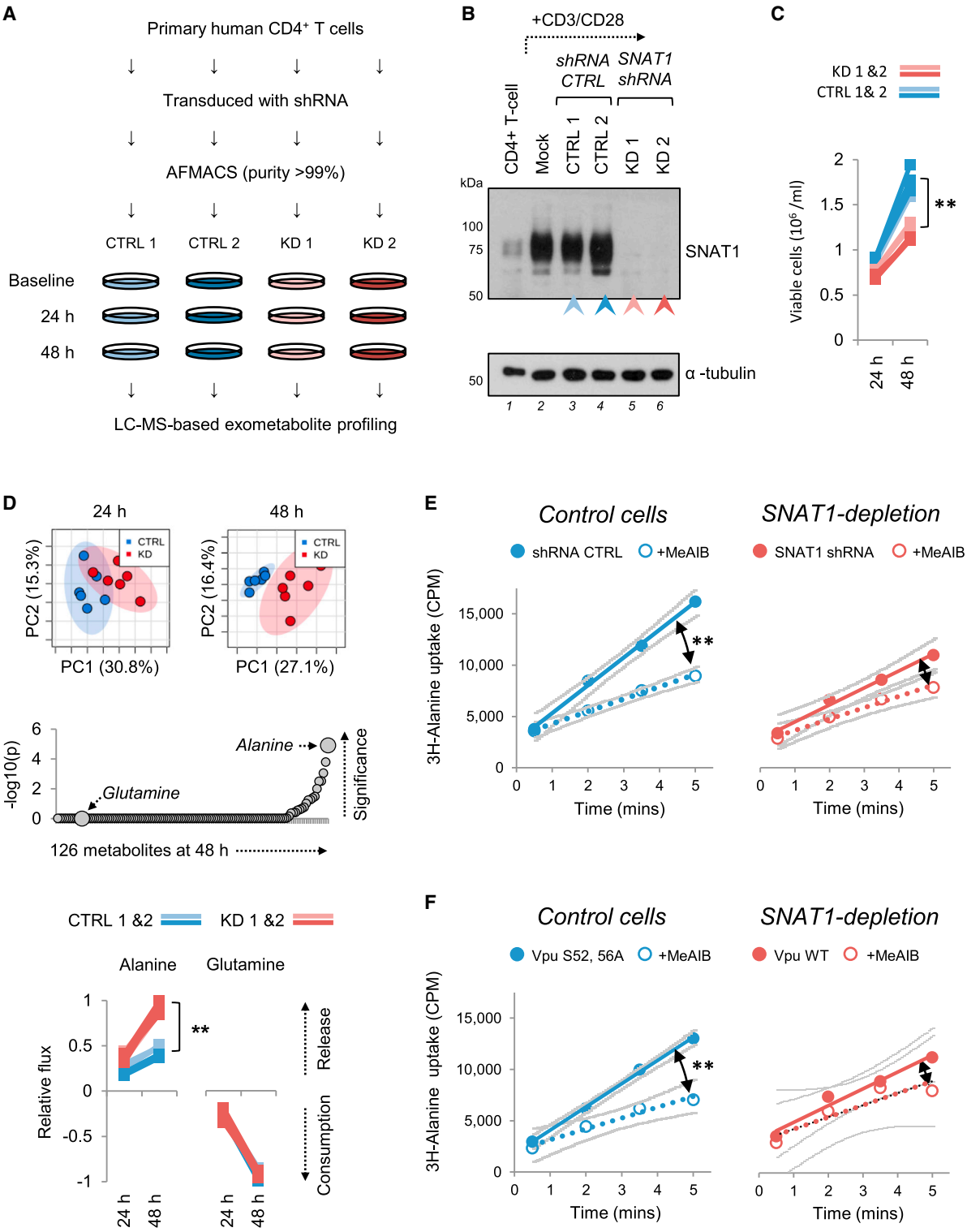

Figure 5. CoRe Metabolomics of Proliferating T Cells and Identification of Alanine Transport by SNAT1

(A) Workflow of CoRe metabolomics experiment.

(B) SNAT1 knockdown for CoRe metabolomics experiment. Primary human CD4+ T cells were activated with CD3/CD28 Dynabeads and mock transduced or transduced with the indicated shRNAs. After purification by AFMACS (Figure S6A), cells were either rested or re-stimulated with CD3/CD28 Dynabeads, then immunoblotted at 48 hr.

(legend continued on next page)

Alanine Transport by Endogenous SNAT1 in T Cells

While attention has focused on glutamine, alanine is the paradigmatic substrate for System A amino acid transport (Oxender and Christensen, 1963) and has consistently been found to be a high-affinity substrate for SNAT1 in overexpression studies (Gu et al., 2001; Mackenzie and Erickson, 2004; Varoqui et al., 2000). We therefore hypothesized that the increase in net alanine release caused by SNAT1 depletion may be explained by a decrease in SNAT1-mediated alanine uptake. To test this, 3H-alanine transport was measured directly in AFMACS-purified primary human CD4+ T cells depleted of SNAT1 by expression of a SNAT1-specific shRNA (Figure 5E) or wild-type Vpu (Figure 5F). Whereas alanine uptake in control T cells was markedly reduced by the System A transport inhibitor MeAIB, this effect was abolished in SNAT1-depleted T cells (Figures 5E and 5F), confirming alanine transport by endogenous SNAT1.

Critical Requirement for Extracellular Alanine in T Cell Mitogenesis

Since alanine is both a non-essential amino acid and excreted by proliferating cells (Jain et al., 2012), including lymphocytes (Figure 5D, lower panels), it appears paradoxical to suggest that a reduction in alanine uptake could result in the mitogenic defect observed in T cells depleted of SNAT1. Nonetheless, we observed a dose-dependent increase in proliferation of CEM-T4 and Jurkat T cells cultured in increasing alanine concentrations (Figure S7A), and a supply of exogenous alanine is required for optimal lymphocyte proliferation in response to PHA (Chuang et al., 1990; Rotter et al., 1979).

We investigated this requirement in primary human CD4+ T cells by activating cells with CD3/CD28 Dynabeads in media supplemented with increasing alanine concentrations. A clear dose response in proliferation from 0 to 0.1 mM was observed (Figure 6A). Furthermore, the effect of increasing alanine concentration was inhibited by MeAIB in a dose-dependent fashion, supporting a role for System A transport in alanine uptake (Figure 6B). Interestingly, exogenous alanine had no effect on the expression of the early T cell activation markers CD69 and CD25 (Figure S7B). The same dissociation of proliferation from early activation has been reported for T cells stimulated in the absence of glutamine (Carr et al., 2010).

Contribution of Extracellular Alanine to the Free Intracellular Amino Acid Pool

To explain the requirement for exogenous alanine in T cell mitogenesis, we hypothesized that bidirectional transport of alanine at the plasma membrane could result in both uptake of extracellular alanine and net alanine excretion (Figure S7C). We therefore measured the size of the free intracellular alanine pool of primary human CD4+ T cells re-stimulated with CD3/CD28 Dynabeads and resuspended in media either lacking alanine or supplemented with a physiological alanine concentration (Figures 6C and S7D). Intracellular alanine levels were markedly reduced by extracellular alanine depletion, but increased by extracellular alanine supplementation, an effect abolished in the presence of MeAIB. These observations confirm bidirectional flux of alanine across the plasma membrane, resulting in equilibration of intracellular and extracellular alanine concentrations, with alanine uptake mediated by System A transport.

The free intracellular alanine pool may be filled by de novo synthesis through transamination of pyruvate, by release of alanine from proteins by proteasomal or lysosomal degradation, or by uptake of extracellular alanine. To formally distinguish these possibilities, and assess their relative contributions, we resuspended washed cells in media supplemented with physiological levels of heavy isotopologue-labeled 13C6-glucose and 15N-alanine (Figure 6D). The free intracellular alanine pool was rapidly reconstituted by extracellular 15N-alanine, an effect markedly inhibited by MeAIB, with little contribution from unlabeled alanine or alanine generated from 13C-glucose-derived pyruvate (Figures 6E and S7D). Conversely, almost all lactate released from cells was derived from glycolysis of 13C6-glucose (Figures 6F). Finally, MeAIB-inhibitable transamination of 15N-alanine to 15N-glutamate was observed (Figure S7E). Extracellular alanine is therefore rapidly taken up by System A transport in primary human CD4+ T cells and incorporated into the wider cellular metabolite pool.

Modulation of T Cell Mitogenesis by SNAT1 Downregulation in HIV-1 Infection

As a functional readout for SNAT1 downregulation in the context of viral infection, we examined the effect of Vpu expression on proliferation of primary human CD4+ T cells. Similar to transduction with SNAT1 shRNA, lentiviral delivery of WT Vpu (but not the Vpu S53, 57A phosphodegron mutant) retarded T cell proliferation (Figure S7F). Remarkably, despite antagonism of cell-cycle progression by Vpr (Malim and Emerman, 2008), and Vpu-independent modulation of a range of mitogenic cell surface proteins (Figure 2E), we also observed a significant reduction in proliferation of T cells infected with WT HIV-1, as compared with Vpu-deficient or Vpu S53, 57A phosphodegron mutant viruses (Figure 6G).

(C) Defective proliferation of SNAT1-depleted primary T cells. Re-stimulated cells from (B) were seeded at equal densities and viable cells enumerated at the indicated time points using CytoCount beads. Data were obtained in triplicate. $^{**}p < 0.01$. No difference in cell size between the two populations was seen by flow cytometry (Figure S6B).

(D) CoRe metabolomic analysis of control and SNAT1-depleted primary T cells. Metabolite compositions of culture supernatants from (C) were determined by LC-MS at baseline, 24, and 48 hr. Data were obtained in triplicate, and Principal component analysis was used to compare net consumption or release of metabolites by control and SNAT1-depleted cells (upper panels). 95% confidence regions are shown. p values for differences in consumption or release of individual metabolites at 48 hr are shown on a negative log scale (middle panel). Net consumption or release of alanine and glutamine is shown scaled to a maximum change of 1 (lower panels). $^{**}p < 0.01$.

(E and F) Impaired alanine uptake by primary T cells depleted of SNAT1 by shRNA (E) or Vpu (F). Cells from Figures 3G–3H were re-stimulated for 48 hr with CD3/CD28 Dynabeads and uptake (counts per minutes; CPM) of 3H-alanine measured at time points from 30 s to 5 min. 3H-alanine transport in the presence of MeAIB is included as a control, and MeAIB-inhibitable uptake is highlighted (black arrows). 95% confidence bands on linear regression lines (indicating rates of uptake) are shown in gray. $^{**}p < 0.01$.

See also Figure S6.

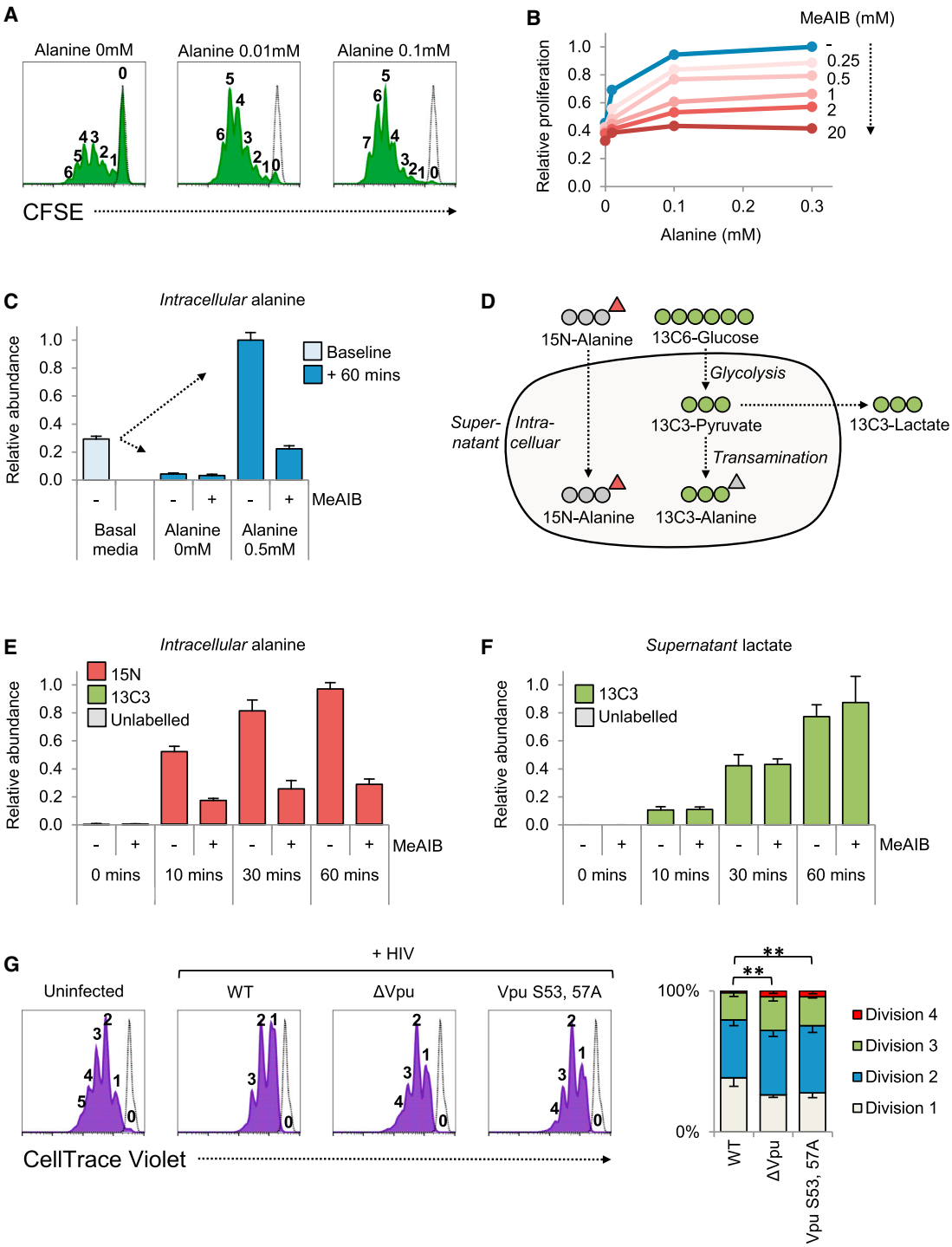

Figure 6. Requirement for Extracellular Alanine in T Cell Mitogenesis

(A) Dose-dependent proliferation of primary T cells in response to exogenous alanine. Primary human CD4+ T cells were stained with CFSE, stimulated with CD3/CD28 Dynabeads in media supplemented with alanine at the concentrations indicated, and analyzed by flow cytometry after 120 hr (green filled histograms). Peaks are labeled by division number, and unstimulated cells were included as a control (black dotted lines). Representative data from three independent experiments are shown.

(B) Dose-dependent inhibition of primary T cell proliferation by MeAIB. Primary human CD4+ T cells were stimulated with CD3/CD28 Dynabeads in media supplemented with alanine and MeAIB at the concentrations indicated. Viable cells were enumerated using CytoCount beads after 72 hr and numbers expressed as a fraction of the maximum.

(C) Regulation of free intracellular alanine pool by System A-dependent alanine uptake. Primary human CD4+ T cells were expanded, rested, and re-stimulated for 48 hr with CD3/CD28 Dynabeads. Cells were then resuspended in media supplemented with alanine at the concentrations indicated in the presence or absence

(legend continued on next page)

SNAT1 Downregulation by Vpu Variants of Pandemic HIV-1 Viruses

HIV-1 viruses form three main groups, each representing a separate transmission of chimpanzee SIVcpz or gorilla SIVgor to humans: M (or Main, responsible for the AIDS pandemic), O (or Outlier), and N (or New or Non-M, Non-O). Group M viruses are responsible for greater than 90% of all HIV infections and cluster into genetically distinct clades, of which the most widespread are A (East Africa), B (Europe and North America), and C (Southern Africa) (Hemelaar et al., 2011). Among non-human primates, Vpu is found in viruses of the SIVcpz lineage (including HIV-1 and SIVgor), as well as more distantly related guenon monkey viruses (SIVgsn, SIVmus, and SIVmon).

To explore the phylogenetic history of Vpu-mediated SNAT1 downregulation, we generated a stable 293T cell line expressing SNAT1-FLAG and CD4 and compared the effects of different Vpu-IRES-GFP constructs. CD4 downregulation is widely conserved and therefore represents a positive control for functional Vpu expression (Sauter et al., 2009). As expected, whereas NL4-3 Vpu (but not Vpu S52A) downregulated both CD4 and SNAT1-FLAG, Nef only downregulated CD4 (Figure 7A). Depletion of cell surface SNAT1-FLAG was conserved across all 6 HIV-1 clade A, B, and C Vpu variants tested (Figures 7A and 7B), but restricted to the SIVcpz *Ptt* lineage giving rise to pandemic HIV-1 group M viruses (Figure 7C). The ability of Vpu to downregulate SNAT1 has therefore been acquired recently and may be critical for the in vivo replication or enhanced pathogenicity of HIV-1 viruses.

DISCUSSION

In this study, we provide a comprehensive, unbiased temporal map of the cell surface of an HIV-1-infected T cell. Our plasma membrane proteomic approach captures transcriptional and post-transcriptional effects, including protein sequestration and redistribution, and is not limited to known T cell immunoreceptors (Weekes et al., 2014). The study of cell surface proteins downregulated by viruses has uncovered important areas of immunobiology, and manipulation by HIV-1 therefore suggests host factors with unsuspected functions in both viral pathogenesis and cellular physiology. Downregulation is unlikely to reflect a non-specific cellular response to productive viral infection because plasma membrane proteins depleted by HIV-1 exhibit contrasting temporal regulation in cells infected with human cytomegalovirus, even within protein families (Figures S1F and S1G) (Weekes et al., 2014).

Along with CD4 and tetherin, our data identify SNAT1 as the third β-TrCP-dependent Vpu substrate. Other Vpu targets have been proposed, based on candidate approaches: NTB-A, CCR7, CD1d, PVR, SELL, and the tetraspanins CD37/53/63/81/82 (Haller et al., 2014; Lambelé et al., 2015; Matusali et al., 2012; Moll et al., 2010; Ramirez et al., 2014; Shah et al., 2010; Vassena et al., 2015). In general, the mechanisms are not β-TrCP dependent, remain poorly characterized, and may be indirect. Furthermore, the magnitude of downregulation reported has been modest, which may contribute to less-robust phenotypes (Sato et al., 2012). Compared with these targets, our systematic analysis suggests that downregulation of CD4, tetherin, and SNAT1 is qualitatively distinct (Figure S3E), reflecting recruitment of β-TrCP and hijack of enzymatic ubiquitin-mediated degradation. Together with downregulation of CD4, MHC-I, SERINC3, and SERINC5 by Nef, we therefore define a more limited group of highly downregulated HIV-1 accessory protein targets.

Vpu and Nef co-operate in the downregulation of CD4 and tetherin, and loss of function in one gene may be compensated by gain of function in the other (Sauter et al., 2009). The Nef proteins of HIV-2 and most SIVs are able to modulate T cell activation by downregulating CD3 from the surface of infected cells, but Nef has lost this ability in most Vpu-containing viruses. Vpu has therefore been suspected to modulate T cell activation via an alternative pathway (Kirchhoff, 2009). We focused on downregulation of SNAT1 both because it is a direct Vpu target and because the importance of amino acid transport in regulating T cell activation is increasingly recognized (Nakaya et al., 2014; Sinclair et al., 2013). Furthermore, while many transporters are poorly characterized multi-pass transmembrane proteins with few reliable reagents, their plasma membrane location makes them potentially druggable therapeutic targets, and inhibitors already exist for many biochemically defined transport systems.

Induction of SNAT1 mRNA correlates with increased glutamine uptake during activation of murine T cells (Carr et al., 2010), but other candidate glutamine transporters are also induced (Nakaya et al., 2014; Wang et al., 2011), and pre-genomic studies attributed lymphocyte glutamine transport to Systems ASC, L, and N, not System A (Segel, 1992). We therefore used an unbiased systematic approach to identify SNAT1 substrates in primary human CD4+ T cells. Measured differences between alanine fluxes of control and SNAT1-depleted cells could potentially reflect both direct transport effects and secondary effects on synthesis or utilization. Alanine may be synthesized by transamination of pyruvate and glutamine-derived glutamate, and re-analysis of data from a previous

of MeAIB. Abundance of free intracellular alanine at baseline and 60 min is expressed as a fraction of the maximum. Mean values and 95% confidence intervals are shown for data obtained in triplicate. No difference in cell size was observed between 0 and 0.5 mM alanine (Figure S7D, left panel).

(D–F) Reconstitution of free intracellular alanine pool by extracellular alanine. Washed cells prepared as in (C) were resuspended in media supplemented with 5.6 mM 13C6-glucose and 0.5 mM 15N-alanine (D) in the presence or absence of MeAIB. Abundances of labeled and unlabeled free intracellular alanine (E) and supernatant lactate (F) at the indicated time points are expressed as a fraction of the maximum. Mean values and 95% confidence intervals are shown for data obtained in triplicate. No difference in cell size was observed in the presence or absence of MeAIB (Figure S7D, right panel).

(G) Defective proliferation of primary T cells depleted of SNAT1 by HIV-1. Primary human CD4+ T cells were stained with CellTrace Violet, stimulated with CD3/CD28 Dynabeads, infected with the indicated NL4-3 Vpu 2_87 HIV-1 viruses at an MOI of 3, and analyzed by flow cytometry after 120 hr (violet filled histograms). Peaks are labeled by division number, and unstimulated cells are included as a control (black dotted lines). Representative data for infected (p24+) and uninfected (p24−) cells are shown. Mean percent of infected cells in each generation from four independent experiments are depicted as stacked columns. Error bars indicate SEM. $^{**}p < 0.01$.

See also Figure S7.

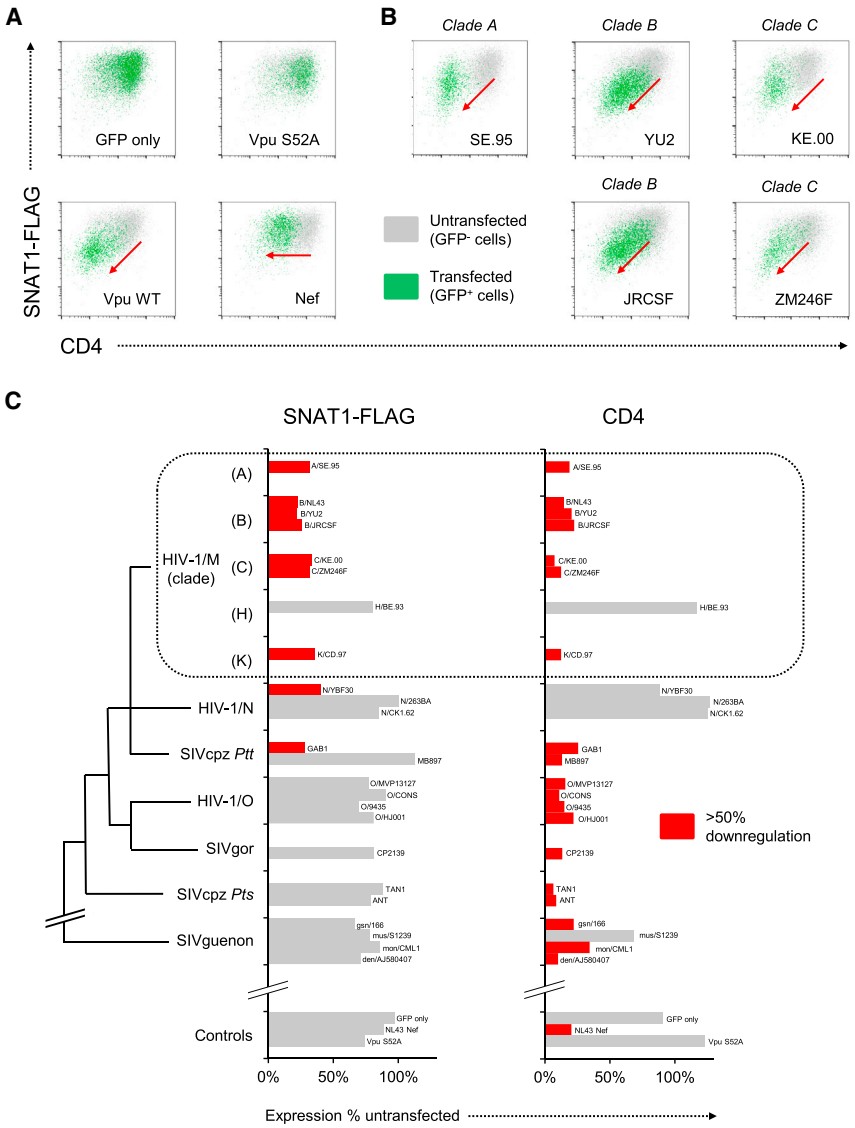

Figure 7. SNAT1 Downregulation by Vpu Variants from Pandemic HIV-1 Viruses

(A) Screening strategy for SNAT1 downregulation by naturally occurring Vpu variants. 293Ts stably expressing SNAT1-FLAG and CD4 were transfected with the indicated pCG-IRES-GFP constructs (all based on HIV-1 group M, clade B, strain NL4-3 virus) and analyzed by flow cytometry at 36 hr. Target downregulation is indicated by a shift in the transfected (GFP^+) cells toward the lower left quadrant (red arrows).

(B) SNAT1-FLAG downregulation by Vpu variants from pandemic HIV-1 group M clade A/B/C viruses. As for (A), but cells were transfected with pCG-IRES-GFP constructs encoding Vpu variants from the indicated strains of HIV-1.

(C) Phylogenetic analysis of SNAT1-FLAG downregulation by Vpu variants of HIV-1 and SIV viruses. As for (A) and (B), but cells were transfected with pCG-IRES-GFP constructs encoding Vpu variants from the indicated strains of HIV-1 or SIV and downregulation of SNAT1-FLAG or CD4 expressed as ratio of geomean fluorescence intensity between transfected (GFP^+) and untransfected (GFP^-) cells. Illustrative phylogenetic relationships are shown, and branch lengths are arbitrary (further details are included in Supplemental Experimental Procedures). HIV-1/M/N/O (HIV-1 group M, N, or O viruses); SIVcpz *Ptt* (SIVs infecting central *P. t. troglodytes* chimpanzees); SIVcpz *Pts* (SIVs infecting eastern *P. t. schweinfruthii* chimpanzees); SIVgor (gorilla SIV); SIVguenon (SIVs infecting guenon monkeys).

CoRe metabolomic screen of NCI-60 cancer cell lines confirmed that release of alanine typically correlates with release of lactate and consumption of glucose and glutamine (Jain et al., 2012). Conversely, we saw no difference between control and SNAT1-depleted cells in release of lactate or consumption of glucose and glutamine (Figures 5D and S6C), suggesting similar rates of alanine synthesis, and confirmed alanine uptake by SNAT1 in primary human CD4+ T cells using a formal transport assay and a concentration of alanine approximating that seen in vivo.

Alanine is the second most abundant amino acid in human plasma, but absent from standard media such as RPMI, and contributed to in vitro cell culture systems by serum supplementation (Rotter et al., 1979). Despite net excretion, we show that the concentration of extracellular alanine dramatically impacts T cell mitogenesis, and uptake of exogenous alanine by System A transport is critical to maintain the free intracellular alanine pool. Alanine is a major constituent of mammalian proteins and may be incorporated into the wider cellular metabolite pool by transamination. In addition, bidirectional transport of alanine at the plasma membrane may be used to drive tertiary active transport of other amino acids (Nicklin et al., 2009). The relative significance of these effects remains to be determined. While amino acid availability is known to regulate immune activation in multiple settings, antagonism of SNAT1 by HIV-1 Vpu is a specific example of viral interference with amino acid immunometabolism.

Modulation of cell surface targets by viruses may enhance viral replication directly, in a cell-autonomous fashion, or indirectly, through effects on non-infected cells or the immune response. It is difficult to account for indirect effects on virus production in vivo using in vitro models. For example, tetherin restricts (Neil et al., 2008) or enhances (Jolly et al., 2010) HIV-1 replication, depending on the assay used. The significance of tetherin as a restriction factor is instead proven by conservation of antagonism across a range of HIV and SIV viruses, and we therefore sought analagous genetic evidence for the importance of SNAT1 in the host-HIV interaction. SNAT1 antagonism was observed for HIV-1 group M Vpu variants from laboratory-adapted viruses and primary patient isolates, including a founder virus strain, X4 and R5 tropic viruses, and related HIV-1 group N and SIVcpz *Ptt* Vpu variants. Remarkably, despite the extraordinary sequence diversity of HIV-1, and the potential to dissociate SNAT1 downregulation from that of CD4 and tetherin, the ability

of Vpu to target SNAT1 is therefore conserved across pandemic HIV-1 viruses, suggesting a significant selective advantage. Furthermore, the restriction of SNAT1 downregulation to Vpu variants from the SIVcpz/HIV-1 lineage suggests a specific role in the pathogenesis of these viruses.

EXPERIMENTAL PROCEDURES

HIV-1 Infections

For proteomic time course analysis, CEM-T4 T cells were spinoculated with VSVg-pseudotyped NL4-3-dE-EGFP HIV-1 virus at an MOI of 10, aliquots of infected cells harvested sequentially at the indicated time points, and dead cells removed by immunomagnetic depletion prior to PMP.

Plasma Membrane Enrichment and Peptide Labeling

PMP was performed as previously described (Weekes et al., 2013, 2014) using 2×10^7 viable cells per condition and a "one pot" oxidation and aminooxy-biotinylation reaction to selectively biotinylate plasma membrane glycoproteins before immunoprecipitation with streptavidin beads and on-bead tryptic digestion. For TMT quantitation, cells from each condition were processed separately, and peptide samples were labeled with TMT reagents before pooling. For SILAC quantitation, cells were pre-labeled by propagation in SILAC media and pooled prior to processing together.

Proteomics and Data Analysis

Peptide samples were fractionated by high-pH reverse-phase high-pressure liquid chromatography (HpRP-HPLC) and analyzed by liquid chromatography coupled to triple-stage (TMT) or tandem (SILAC) mass spectrometry using an Orbitrap Fusion Tribrid (TMT) or Q Exactive (SILAC) mass spectrometer. Reporter ions from TMT-labeled peptides were quantitated from an MS3 scan using Proteome Discoverer. SILAC-labeled peptides were quantitated using MaxQuant.

Primary Cell Knockdowns

Primary human CD4+ T cells were activated with CD3/CD28 Dynabeads and transduced with lentiviral constructs encoding U6-shRNA knockdown and SFFV-SBP-ΔLNGFR streptavidin-binding affinity tag cassettes. Transduced cells were selected with streptavidin Dynabeads then released by incubation with excess biotin as previously described (AFMACS) (Matheson et al., 2014). Ethical permission for this project was granted by the Cambridgeshire 2 Research Ethics Committee (REC reference 97/092). Informed written consent was obtained from all of the volunteers included in this study prior to providing blood samples.

CoRe Metabolomics and Data Analysis

AFMACS-purified primary human CD4+ T cells expressing control or SNAT1-specific shRNAs were re-stimulated using CD3/CD28 Dynabeads. After 24 hr, cells were resuspended in 20% conditioned media at equal densities and supernatant samples at baseline, 24, and 48 hr were analyzed by liquid chromatography coupled to mass spectrometry (LC-MS) as previously described (Jain et al., 2012). To account for differential proliferation, viable cells were enumerated at each time point and changes in metabolite concentrations normalized based on average cell numbers.

3H-Alanine Uptake

AFMACS-purified primary human CD4+ T cells expressing control or SNAT1-specific shRNAs were re-stimulated using CD3/CD2 min8 Dynabeads. After 48 hr, cells were starved to reduce *trans*-inhibition then resuspended at 37°C in Tyrode's buffer supplemented with 3H-alanine at a final concentration of 0.5 mM. Aliquots of cells were harvested sequentially over 5 min and uptake terminated by filtering centrifugation through silicone oil before liquid scintillation counting.

Free Intracellular Amino Acids

Primary human CD4+ T cells were expanded once and then re-stimulated using CD3/CD28 Dynabeads. After 48 hr, cells were resuspended in media supplemented with dialyzed FCS and either unlabeled alanine and glucose or (for stable isotopologue-resolved metabolomics) 15N-alanine and 13C6-glucose at concentrations of 0.5 mM and 5.6 mM, respectively. Aliquots of cells were harvested sequentially over 1 hr, and free intracellular amino acids were extracted from washed cells using dry ice-cold 50% methanol 30% acetonitrile before analysis by LC-MS. Please see Supplemental Experimental Procedures for further details.

SUPPLEMENTAL INFORMATION

Supplemental Information includes Supplemental Experimental Procedures, seven figures, and three tables and can be found with this article online at http://dx.doi.org/10.1016/j.chom.2015.09.003.

AUTHOR CONTRIBUTIONS

N.J.M. and P.J.L. conceived the project and wrote the manuscript; N.J.M., J.S., K.W., R.R., M.P.W., R.V., and J.W. performed experiments; M.P.W. and N.J.M. developed proteomic methods; M.S. supplied essential reagents; R.A. conducted proteomic mass spectrometry; A.S.H.C., C.F., and C.B.C. conducted metabolomic mass spectrometry; and S.J.D.N. and P.J.L. supervised the project. J.S., K.W., and R.R. contributed equally to the final manuscript.

ACKNOWLEDGMENTS

This work was supported by a Wellcome Trust PRF (WT101835) to P.J.L. and SRF (WT098049) to S.J.D.N., the NIHR Cambridge BRC, a Wellcome Trust Strategic Award to CIMR, and the Addenbrooke's Charitable Trust. M.P.W. is a Wellcome Trust Fellow (093966/Z/10/Z), and N.J.M. is a Wellcome Trust Training Fellow (093964/Z/10/Z) and Raymond and Beverly Sackler student. The authors thank Dr. Jenny Ho (Thermo) for help with proteomics, Dr. Jo Glazier (University of Manchester) and Dr. Richard Boyd (University of Oxford) for advice on amino acid transport assays, Dr. Reiner Schulte and his team for FACS, Matthew Gratian and Mark Bowen for microscopy, and the Lehner laboratory for critical discussion.

Received: July 2, 2015
Revised: August 30, 2015
Accepted: September 10, 2015
Published: October 1, 2015

REFERENCES

Abraham, L., and Fackler, O.T. (2012). HIV-1 Nef: a multifaceted modulator of T cell receptor signaling. Cell Commun. Signal. *10*, 39.

Brandt, C.S., Baratin, M., Yi, E.C., Kennedy, J., Gao, Z., Fox, B., Haldeman, B., Ostrander, C.D., Kaifu, T., Chabannon, C., et al. (2009). The B7 family member B7-H6 is a tumor cell ligand for the activating natural killer cell receptor NKp30 in humans. J. Exp. Med. *206*, 1495–1503.

Carr, E.L., Kelman, A., Wu, G.S., Gopaul, R., Senkevitch, E., Aghvanyan, A., Turay, A.M., and Frauwirth, K.A. (2010). Glutamine uptake and metabolism are coordinately regulated by ERK/MAPK during T lymphocyte activation. J. Immunol. *185*, 1037–1044.

Chaudhry, F.A., Reimer, R.J., and Edwards, R.H. (2002). The glutamine commute: take the N line and transfer to the A. J. Cell Biol. *157*, 349–355.

Chuang, J.C., Yu, C.L., and Wang, S.R. (1990). Modulation of human lymphocyte proliferation by amino acids. Clin. Exp. Immunol. *81*, 173–176.

Douglas, J.L., Viswanathan, K., McCarroll, M.N., Gustin, J.K., Früh, K., and Moses, A.V. (2009). Vpu directs the degradation of the human immunodeficiency virus restriction factor BST-2/Tetherin via a betaTrCP-dependent mechanism. J. Virol. *83*, 7931–7947.

Gu, S., Roderick, H.L., Camacho, P., and Jiang, J.X. (2001). Characterization of an N-system amino acid transporter expressed in retina and its involvement in glutamine transport. J. Biol. Chem. *276*, 24137–24144.

Haller, C., Müller, B., Fritz, J.V., Lamas-Murua, M., Stolp, B., Pujol, F.M., Keppler, O.T., and Fackler, O.T. (2014). HIV-1 Nef and Vpu are functionally

redundant broad-spectrum modulators of cell surface receptors, including tetraspanins. J. Virol. *88*, 14241–14257.

Hemelaar, J., Gouws, E., Ghys, P.D., and Osmanov, S.; WHO-UNAIDS Network for HIV Isolation and Characterisation (2011). Global trends in molecular epidemiology of HIV-1 during 2000-2007. AIDS *25*, 679–689.

Hout, D.R., Gomez, M.L., Pacyniak, E., Gomez, L.M., Inbody, S.H., Mulcahy, E.R., Culley, N., Pinson, D.M., Powers, M.F., Wong, S.W., and Stephens, E.B. (2005). Scrambling of the amino acids within the transmembrane domain of Vpu results in a simian-human immunodeficiency virus (SHIVTM) that is less pathogenic for pig-tailed macaques. Virology *339*, 56–69.

Jain, M., Nilsson, R., Sharma, S., Madhusudhan, N., Kitami, T., Souza, A.L., Kafri, R., Kirschner, M.W., Clish, C.B., and Mootha, V.K. (2012). Metabolite profiling identifies a key role for glycine in rapid cancer cell proliferation. Science *336*, 1040–1044.

Jolly, C., Booth, N.J., and Neil, S.J. (2010). Cell-cell spread of human immunodeficiency virus type 1 overcomes tetherin/BST-2-mediated restriction in T cells. J. Virol. *84*, 12185–12199.

Keele, B.F., Jones, J.H., Terio, K.A., Estes, J.D., Rudicell, R.S., Wilson, M.L., Li, Y., Learn, G.H., Beasley, T.M., Schumacher-Stankey, J., et al. (2009). Increased mortality and AIDS-like immunopathology in wild chimpanzees infected with SIVcpz. Nature *460*, 515–519.

Kirchhoff, F. (2009). Is the high virulence of HIV-1 an unfortunate coincidence of primate lentiviral evolution? Nat. Rev. Microbiol. *7*, 467–476.

Lambelé, M., Koppensteiner, H., Symeonides, M., Roy, N.H., Chan, J., Schindler, M., and Thali, M. (2015). Vpu is the main determinant for tetraspanin downregulation in HIV-1-infected cells. J. Virol. *89*, 3247–3255.

Mackenzie, B., and Erickson, J.D. (2004). Sodium-coupled neutral amino acid (System N/A) transporters of the SLC38 gene family. Pflugers Arch. *447*, 784–795.

Malim, M.H., and Emerman, M. (2008). HIV-1 accessory proteins–ensuring viral survival in a hostile environment. Cell Host Microbe *3*, 388–398.

Margottin, F., Bour, S.P., Durand, H., Selig, L., Benichou, S., Richard, V., Thomas, D., Strebel, K., and Benarous, R. (1998). A novel human WD protein, h-beta TrCp, that interacts with HIV-1 Vpu connects CD4 to the ER degradation pathway through an F-box motif. Mol. Cell *1*, 565–574.

Matheson, N.J., Peden, A.A., and Lehner, P.J. (2014). Antibody-free magnetic cell sorting of genetically modified primary human CD4+ T cells by one-step streptavidin affinity purification. PLoS ONE *9*, e111437.

Matta, J., Baratin, M., Chiche, L., Forel, J.M., Cognet, C., Thomas, G., Farnarier, C., Piperoglou, C., Papazian, L., Chaussabel, D., et al. (2013). Induction of B7-H6, a ligand for the natural killer cell-activating receptor NKp30, in inflammatory conditions. Blood *122*, 394–404.

Matusali, G., Potestà, M., Santoni, A., Cerboni, C., and Doria, M. (2012). The human immunodeficiency virus type 1 Nef and Vpu proteins downregulate the natural killer cell-activating ligand PVR. J. Virol. *86*, 4496–4504.

Mitchell, R.S., Katsura, C., Skasko, M.A., Fitzpatrick, K., Lau, D., Ruiz, A., Stephens, E.B., Margottin-Goguet, F., Benarous, R., and Guatelli, J.C. (2009). Vpu antagonizes BST-2-mediated restriction of HIV-1 release via beta-TrCP and endo-lysosomal trafficking. PLoS Pathog. *5*, e1000450.

Moll, M., Andersson, S.K., Smed-Sörensen, A., and Sandberg, J.K. (2010). Inhibition of lipid antigen presentation in dendritic cells by HIV-1 Vpu interference with CD1d recycling from endosomal compartments. Blood *116*, 1876–1884.

Monroe, K.M., Yang, Z., Johnson, J.R., Geng, X., Doitsh, G., Krogan, N.J., and Greene, W.C. (2014). IFI16 DNA sensor is required for death of lymphoid CD4 T cells abortively infected with HIV. Science *343*, 428–432.

Nakaya, M., Xiao, Y., Zhou, X., Chang, J.H., Chang, M., Cheng, X., Blonska, M., Lin, X., and Sun, S.C. (2014). Inflammatory T cell responses rely on amino acid transporter ASCT2 facilitation of glutamine uptake and mTORC1 kinase activation. Immunity *40*, 692–705.

Neil, S.J., Zang, T., and Bieniasz, P.D. (2008). Tetherin inhibits retrovirus release and is antagonized by HIV-1 Vpu. Nature *451*, 425–430.

Nicklin, P., Bergman, P., Zhang, B., Triantafellow, E., Wang, H., Nyfeler, B., Yang, H., Hild, M., Kung, C., Wilson, C., et al. (2009). Bidirectional transport of amino acids regulates mTOR and autophagy. Cell *136*, 521–534.

Oxender, D.L., and Christensen, H.N. (1963). Evidence for two types of mediation of neutral and amino-acid transport in Ehrlich cells. Nature *197*, 765–767.

Ramirez, P.W., Famiglietti, M., Sowrirajan, B., DePaula-Silva, A.B., Rodesch, C., Barker, E., Bosque, A., and Planelles, V. (2014). Downmodulation of CCR7 by HIV-1 Vpu results in impaired migration and chemotactic signaling within $CD4^+$ T cells. Cell Rep. *7*, 2019–2030.

Rotter, V., Yakir, Y., and Trainin, N. (1979). Role of L-alanine in the response of human lymphocytes to PHA and Con A. J. Immunol. *123*, 1726–1731.

Sato, K., Misawa, N., Fukuhara, M., Iwami, S., An, D.S., Ito, M., and Koyanagi, Y. (2012). Vpu augments the initial burst phase of HIV-1 propagation and downregulates BST2 and CD4 in humanized mice. J. Virol. *86*, 5000–5013.

Sauter, D., Schindler, M., Specht, A., Landford, W.N., Münch, J., Kim, K.A., Votteler, J., Schubert, U., Bibollet-Ruche, F., Keele, B.F., et al. (2009). Tetherin-driven adaptation of Vpu and Nef function and the evolution of pandemic and nonpandemic HIV-1 strains. Cell Host Microbe *6*, 409–421.

Schindler, M., Münch, J., Kutsch, O., Li, H., Santiago, M.L., Bibollet-Ruche, F., Müller-Trutwin, M.C., Novembre, F.J., Peeters, M., Courgnaud, V., et al. (2006). Nef-mediated suppression of T cell activation was lost in a lentiviral lineage that gave rise to HIV-1. Cell *125*, 1055–1067.

Schubert, U., Antón, L.C., Bacík, I., Cox, J.H., Bour, S., Bennink, J.R., Orlowski, M., Strebel, K., and Yewdell, J.W. (1998). CD4 glycoprotein degradation induced by human immunodeficiency virus type 1 Vpu protein requires the function of proteasomes and the ubiquitin-conjugating pathway. J. Virol. *72*, 2280–2288.

Segel, G.B. (1992). Amino Acid Transport in Lymphocytes. In Mammalian Amino Acid Transport, M.S. Kilberg and D. Haussinger, eds. (Springer), pp. 261–274.

Shah, A.H., Sowrirajan, B., Davis, Z.B., Ward, J.P., Campbell, E.M., Planelles, V., and Barker, E. (2010). Degranulation of natural killer cells following interaction with HIV-1-infected cells is hindered by downmodulation of NTB-A by Vpu. Cell Host Microbe *8*, 397–409.

Sinclair, L.V., Rolf, J., Emslie, E., Shi, Y.B., Taylor, P.M., and Cantrell, D.A. (2013). Control of amino-acid transport by antigen receptors coordinates the metabolic reprogramming essential for T cell differentiation. Nat. Immunol. *14*, 500–508.

Singh, D.K., Griffin, D.M., Pacyniak, E., Jackson, M., Werle, M.J., Wisdom, B., Sun, F., Hout, D.R., Pinson, D.M., Gunderson, R.S., et al. (2003). The presence of the casein kinase II phosphorylation sites of Vpu enhances the CD4(+) T cell loss caused by the simian-human immunodeficiency virus SHIV(KU-1bMC33) in pig-tailed macaques. Virology *313*, 435–451.

Stephens, E.B., McCormick, C., Pacyniak, E., Griffin, D., Pinson, D.M., Sun, F., Nothnick, W., Wong, S.W., Gunderson, R., Berman, N.E., and Singh, D.K. (2002). Deletion of the vpu sequences prior to the env in a simian-human immunodeficiency virus results in enhanced Env precursor synthesis but is less pathogenic for pig-tailed macaques. Virology *293*, 252–261.

Swigut, T., Shohdy, N., and Skowronski, J. (2001). Mechanism for down-regulation of CD28 by Nef. EMBO J. *20*, 1593–1604.

Tokarev, A., and Guatelli, J. (2011). Misdirection of membrane trafficking by HIV-1 Vpu and Nef: Keys to viral virulence and persistence. Cell. Logist. *1*, 90–102.

Varoqui, H., Zhu, H., Yao, D., Ming, H., and Erickson, J.D. (2000). Cloning and functional identification of a neuronal glutamine transporter. J. Biol. Chem. *275*, 4049–4054.

Vassena, L., Giuliani, E., Koppensteiner, H., Bolduan, S., Schindler, M., and Doria, M. (2015). HIV-1 Nef and Vpu Interfere with L-Selectin (CD62L) Cell Surface Expression To Inhibit Adhesion and Signaling in Infected CD4+ T Lymphocytes. J. Virol. *89*, 5687–5700.

Vigan, R., and Neil, S.J. (2010). Determinants of tetherin antagonism in the transmembrane domain of the human immunodeficiency virus type 1 Vpu protein. J. Virol. *84*, 12958–12970.

Wang, R., Dillon, C.P., Shi, L.Z., Milasta, S., Carter, R., Finkelstein, D., McCormick, L.L., Fitzgerald, P., Chi, H., Munger, J., and Green, D.R. (2011). The transcription factor Myc controls metabolic reprogramming upon T lymphocyte activation. Immunity *35*, 871–882.

Weekes, M.P., Tan, S.Y., Poole, E., Talbot, S., Antrobus, R., Smith, D.L., Montag, C., Gygi, S.P., Sinclair, J.H., and Lehner, P.J. (2013). Latency-associated degradation of the MRP1 drug transporter during latent human cytomegalovirus infection. Science *340*, 199–202.

Weekes, M.P., Tomasec, P., Huttlin, E.L., Fielding, C.A., Nusinow, D., Stanton, R.J., Wang, E.C., Aicheler, R., Murrell, I., Wilkinson, G.W., et al. (2014). Quantitative temporal viromics: an approach to investigate host-pathogen interaction. Cell *157*, 1460–1472.

Zhang, F., Wilson, S.J., Landford, W.C., Virgen, B., Gregory, D., Johnson, M.C., Munch, J., Kirchhoff, F., Bieniasz, P.D., and Hatziioannou, T. (2009). Nef proteins from simian immunodeficiency viruses are tetherin antagonists. Cell Host Microbe *6*, 54–67.

Cell Host & Microbe, Volume *18*

Supplemental Information

Cell Surface Proteomic Map of HIV Infection Reveals Antagonism of Amino Acid Metabolism by Vpu and Nef

Nicholas J. Matheson, Jonathan Sumner, Kim Wals, Radu Rapiteanu, Michael P. Weekes, Raphael Vigan, Julia Weinelt, Michael Schindler, Robin Antrobus, Ana S.H. Costa, Christian Frezza, Clary B. Clish, Stuart J.D. Neil, and Paul J. Lehner

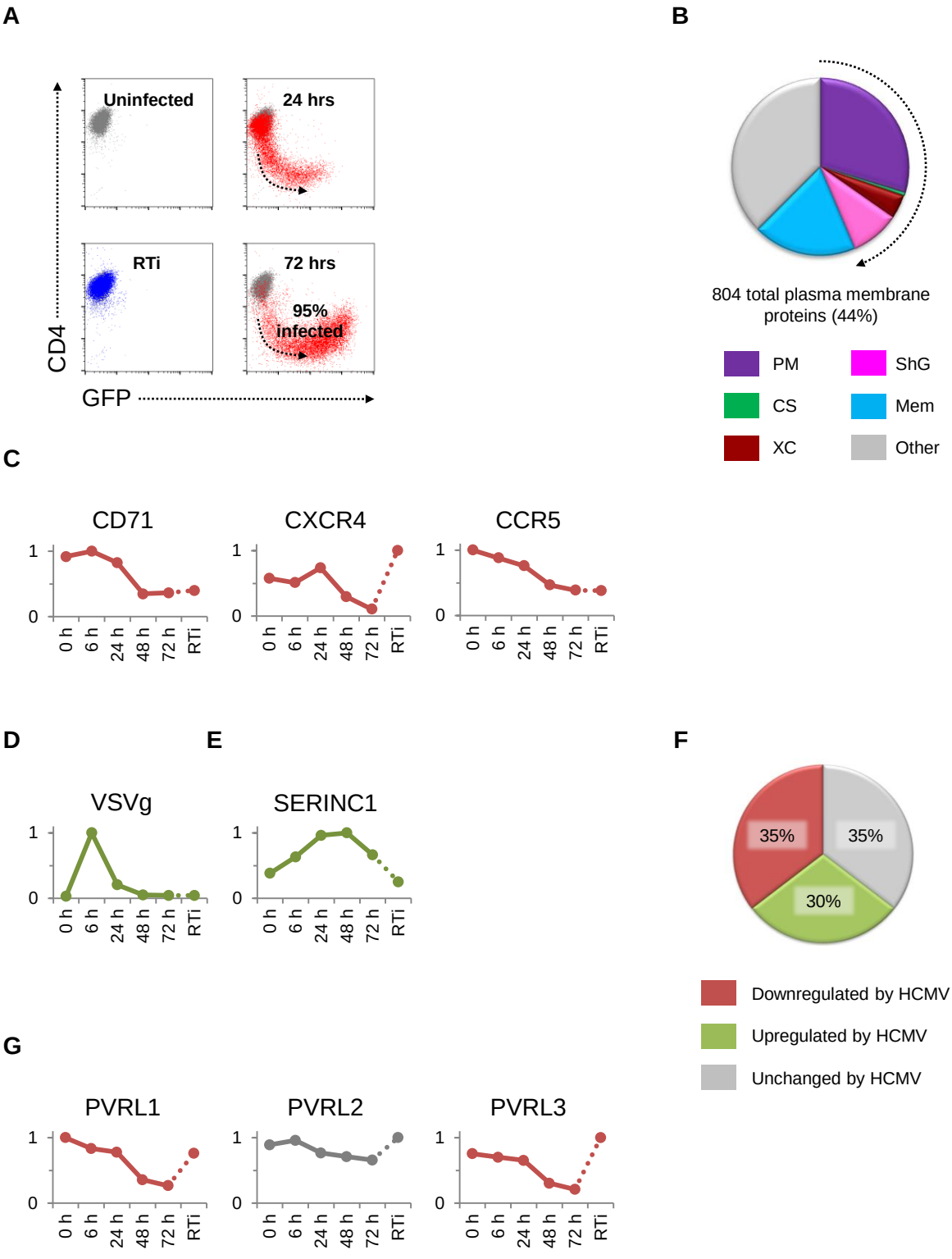

Figure S1. Controls for TMT-based Proteomic Timecourse and Comparison with HCMV Infection, Related to Figure 1

(A) Identification of HIV-infected cells. Cells from **Figure 1A** were stained with anti-CD4 antibody and analysed by flow cytometry. Productive infection with VSVg-pseudotyped NL4-

3-deltaE-EGFP virus results in expression of GFP and downregulation of CD4 by Nef and Vpu. Uninfected cells (grey), cells infected for 24 and 72 hrs (red) and cells infected for 72 hrs in the presence of reverse transcriptase inhibitors (blue) are shown.

(B) Gene Ontology Cellular Compartment (GOCC) annotation of quantitated proteins. PM, plasma membrane; CS, cell surface; XC, extracellular; ShG, short GOCC (a subset of proteins with short membrane-specific GOCC terms but no subcellular assignment (Weekes et al., 2012); Mem, membrane. 1,846 of 2,320 quantitated proteins had GOCC annotations, of which 804 (44%) were indicative of plasma membrane localisation.

(C) Temporal profiles of other reported targets for HIV-mediated downregulation (Drakesmith et al., 2005; Koppensteiner et al., 2014; Michel et al., 2006; Ramirez et al., 2014).

(D) Temporal profile of VSVg.

(E) Temporal profile of SERINC1.

(F) Differential regulation of cell surface proteins by HIV and HCMV infection. 79 proteins from Cluster #35 (cell surface proteins progressively downregulated by HIV) were previously quantitated in HCMV-infected fibroblasts (Weekes et al., 2014) and found to be variably upregulated, downregulated, or unchanged by HCMV infection.

(G) Temporal profiles of nectins (PVRL1-3) revealing differential regulation by HIV and HCMV. Nectin-2 (PVRL2, CD112) is targeted for proteasomal degradation by co-operation between the HCMV proteins UL141 and US2. Conversely, in HIV-1-infected cells (as shown), we observed downregulation of nectin-1 (PVRL1, CD111) and nectin-3 (PVRL3, CD113), but not nectin-2.

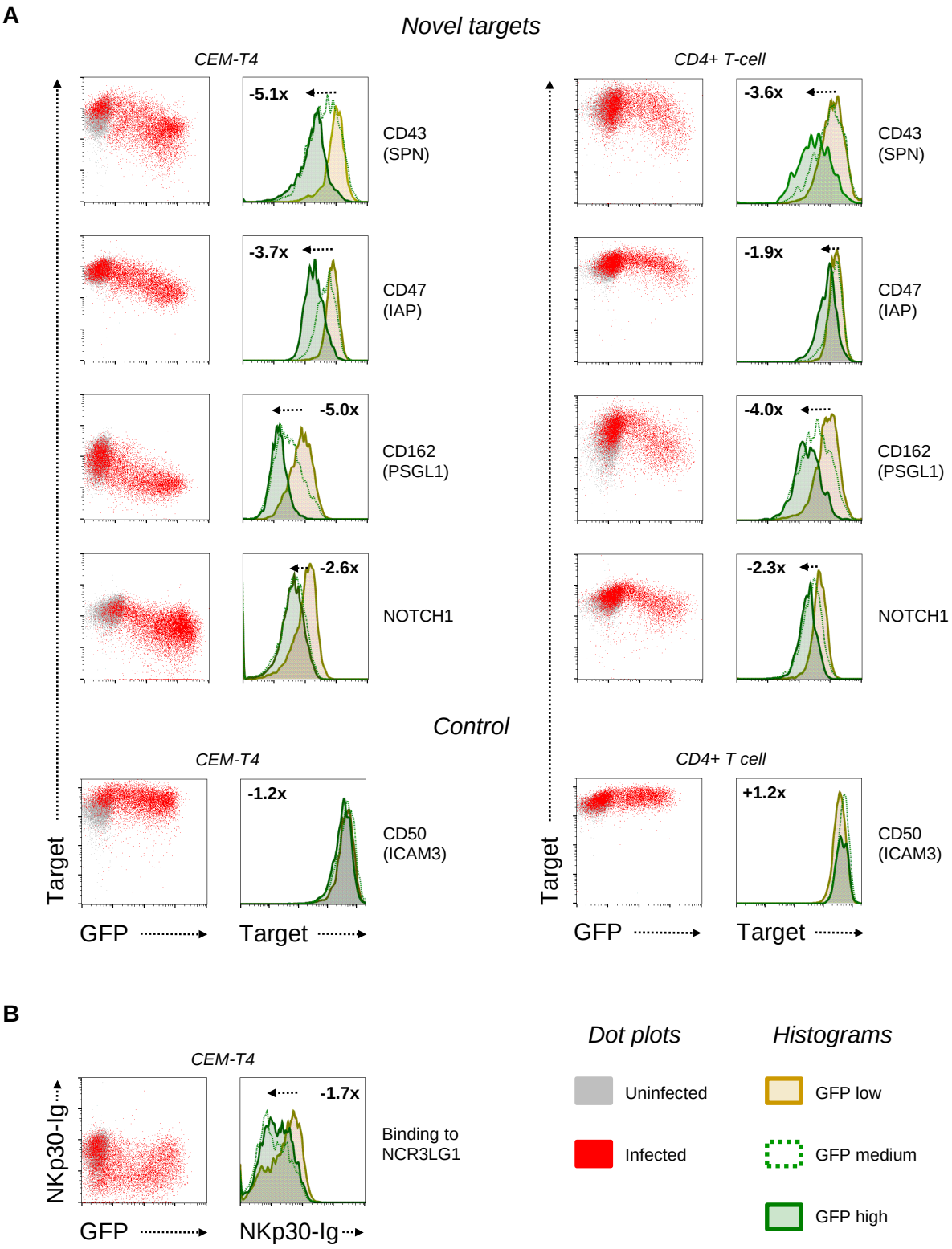

Figure S2. Flow Cytometric Validation of Novel HIV-1 Targets, Related to Figure 2

(A) Validation of novel HIV-1 targets by flow cytometry in CEM-T4s and primary T-cells. CEM-T4s or primary human CD4+ T-cells stimulated with CD3/CD28 Dynabeads were stained with antibodies against the indicated targets 48 hrs after infection with NL4-3-deltaE-

EGFP HIV-1 virus typically at an MOI of 1. Target expression is shown for GFP low, medium and high cells and fold-change in geomean fluorescence intensity high/low is indicated. Negative values denote downregulation in productively infected (GFP-expressing) cells. CD50 abundance was unchanged by HIV-infection in the TMT dataset and is included as a control.

(B) Downregulation of NCR3LG1. CEM-T4s were stained with NKp30-Ig fusion protein (endogenous NCR3LG1 ligand) 48 hrs after infection with NL4-3-deltaE-EGFP HIV-1 virus at an MOI of 1. As in (A) NKp30-Ig binding is shown for GFP low, medium and high cells and fold-change high/low is indicated.

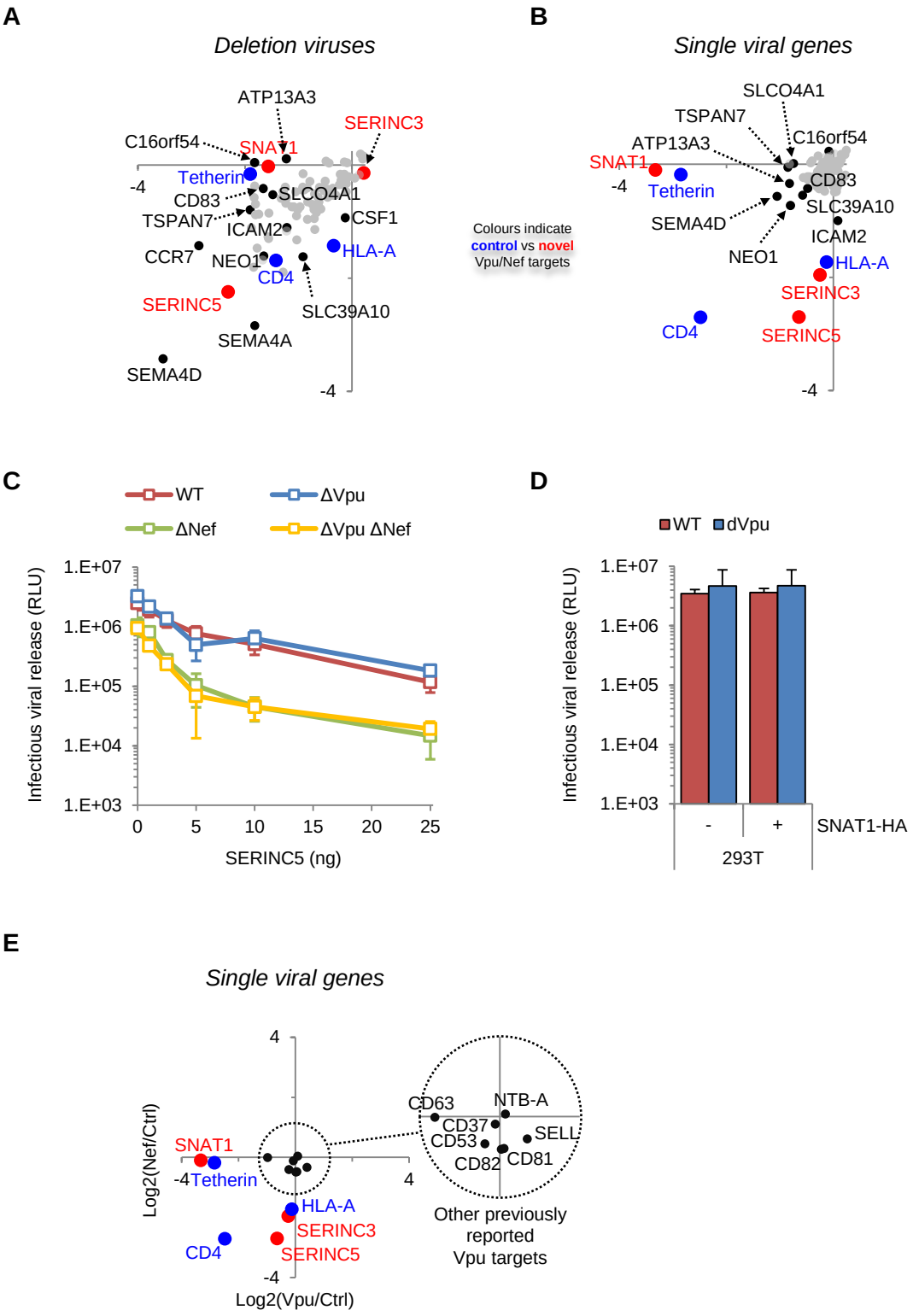

Figure S3. Novel Vpu and Nef targets, Related to Figure 3

(A-B) SILAC-based quantitation of plasma membrane proteins in cells infected with Vpu-deficient (y-axis) versus Nef-deficient (x-axis) viruses (A; enlarged left lower quadrant of scatterplot shown in **Figure 3A**) or transduced with Vpu (x-axis) versus Nef (y-axis) as single

genes (B; enlarged left lower quadrant of scatterplot shown in **Figure 3B**). Outliers of potential interest are labelled.

(C) Restriction of HIV-1 virus production by SERINC5. 293Ts were co-transfected with the indicated pNL4-3 HIV-1 molecular clones plus increasing concentrations of pCR3.1-SERINC5 and 48 hr culture supernatants assayed for infectious viral release using HeLa-TZM-bl cells. Mean values and 95% confidence intervals are shown.

(D) No effect on HIV-1 virus production by SNAT1. Control and SNAT1-HA-expressing 293Ts were infected with the indicated VSVg-pseudotyped NL4-3 HIV-1 viruses at an MOI of 2 and 48 hr culture supernatants assayed for infectious virus release using HeLa-TZM-bl cells. Mean values and 95% confidence intervals are shown.

(E) Comparison of SNAT1 with known Vpu targets. As for (B) and Figure 3B, but showing downregulation of SNAT1, CD4 and tetherin compared with previously reported Vpu targets NTB-A, SELL, CD37, CD53, CD63, CD81 and CD82. HLA-A (downregulated by Nef) is also shown. CCR7, CD1d and PVR (CD155) were not quantitated in this experiment, but CCR7 was downregulated by both ΔVpu and ΔNef viruses. CD53 was quantitated on the basis of a single PSM.

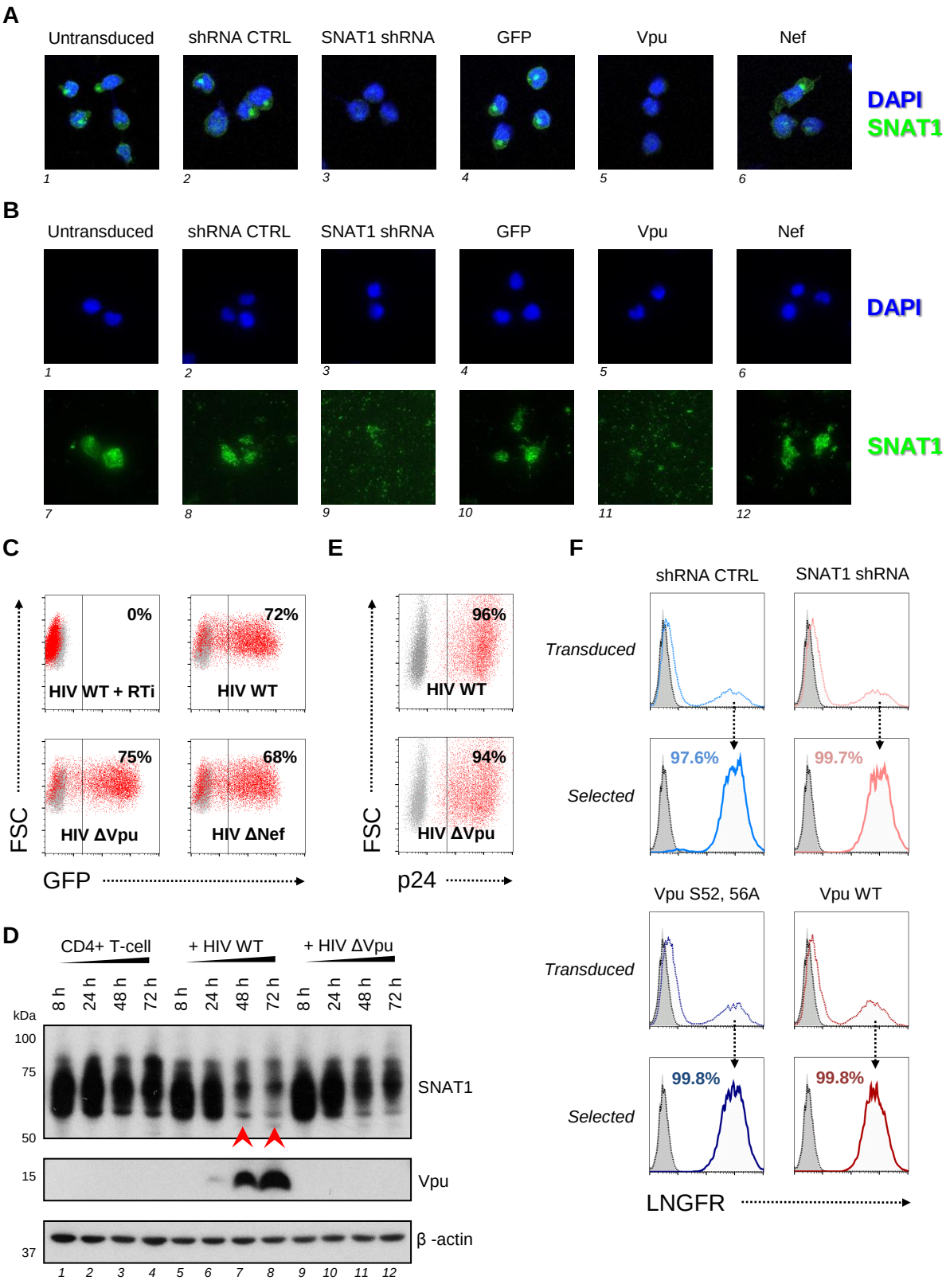

Figure S4. Validation of SNAT1 Depletion, Related to Figure 3

(A-B) Cell surface SNAT1 depletion by Vpu. Cells from **Figure 3E** were stained with anti-SNAT1 antibody (green) and DAPI (blue) and analysed by confocal microscopy (A) or TIRF

microscopy (B). TIRF microscopy enables selective visualisation of the plasma membrane (SNAT1; lower panels) with widefield images (DAPI; upper panels) included as controls.

(C) Infection controls for **Figures 3C-D**. Cells from **Figures 3C-D** were analysed by flow cytometry 48 hrs after infection with the indicated NL4-3-deltaE-EGFP HIV-1 viruses. In each case % productively infected (GFP+) cells is indicated. Uninfected cells (grey) are also shown.

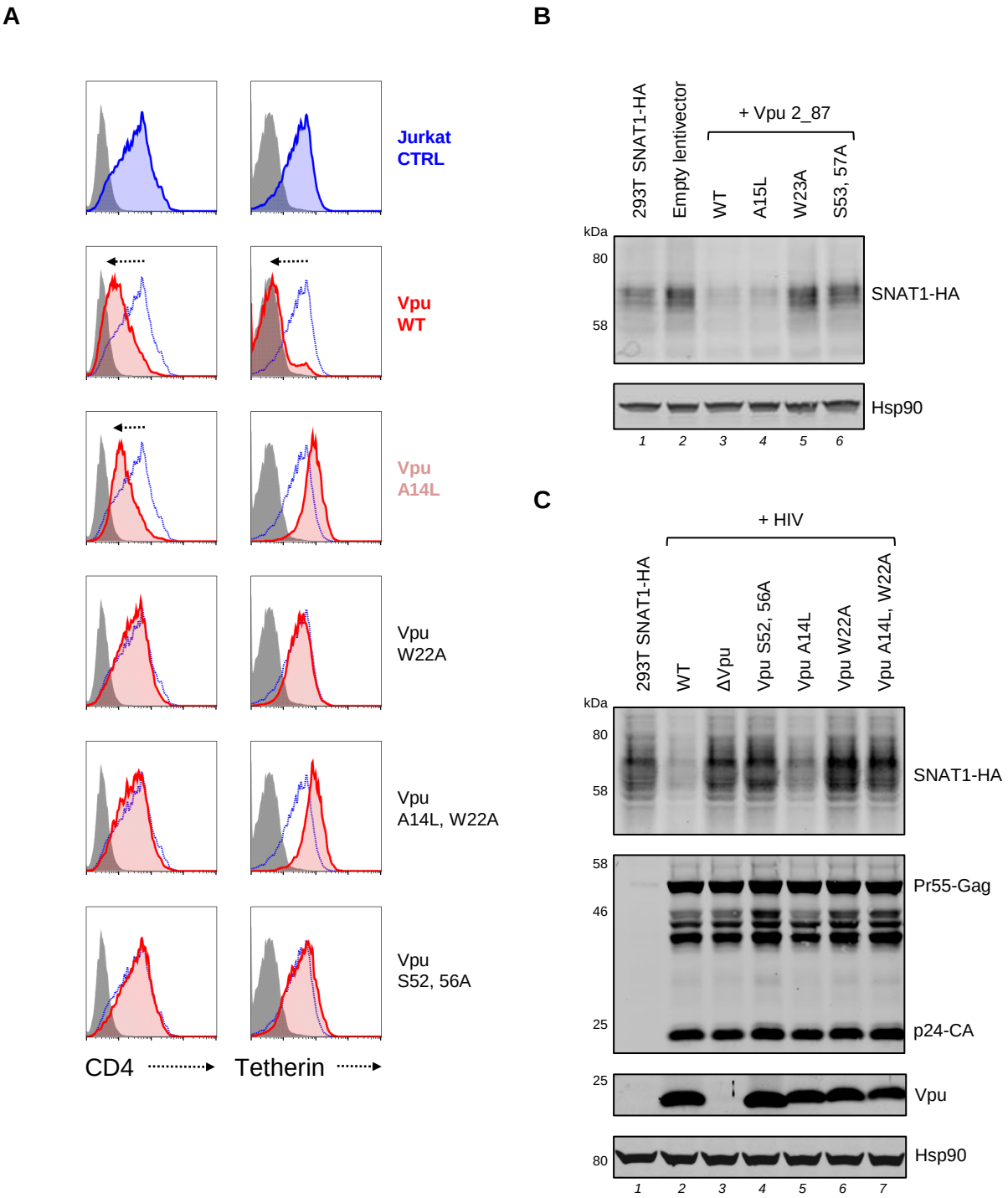

Figure S5. Controls for Mechanism of SNAT1 Depletion, Related to Figure 4

(A) Molecular determinants of CD4 and tetherin downregulation. Cells from **Figure 4F** were stained with anti-CD4 or anti-tetherin antibodies and analysed by flow cytometry. Jurkats transduced with empty vector (blue) or Vpu variants (red) are shown. Unstained cells (CD4) or cells stained with secondary antibody only (tetherin) are included as controls (grey).

(B) Depletion of SNAT1 by Vpu 2_87. 293Ts stably expressing SNAT1-HA were transduced with the indicated Vpu constructs at an MOI of 2 then immunoblotted with anti-HA and HSP90 (loading control) antibodies.

(C) Molecular determinants of SNAT1 depletion by HIV-1. 293Ts stably expressing SNAT1-HA were infected with the indicated VSVg-pseudotyped NL4-3 HIV-1 viruses at an MOI of 2 then immunoblotted with anti-HA, anti-p24, anti-Vpu and anti-HSP90 (loading control) antibodies.

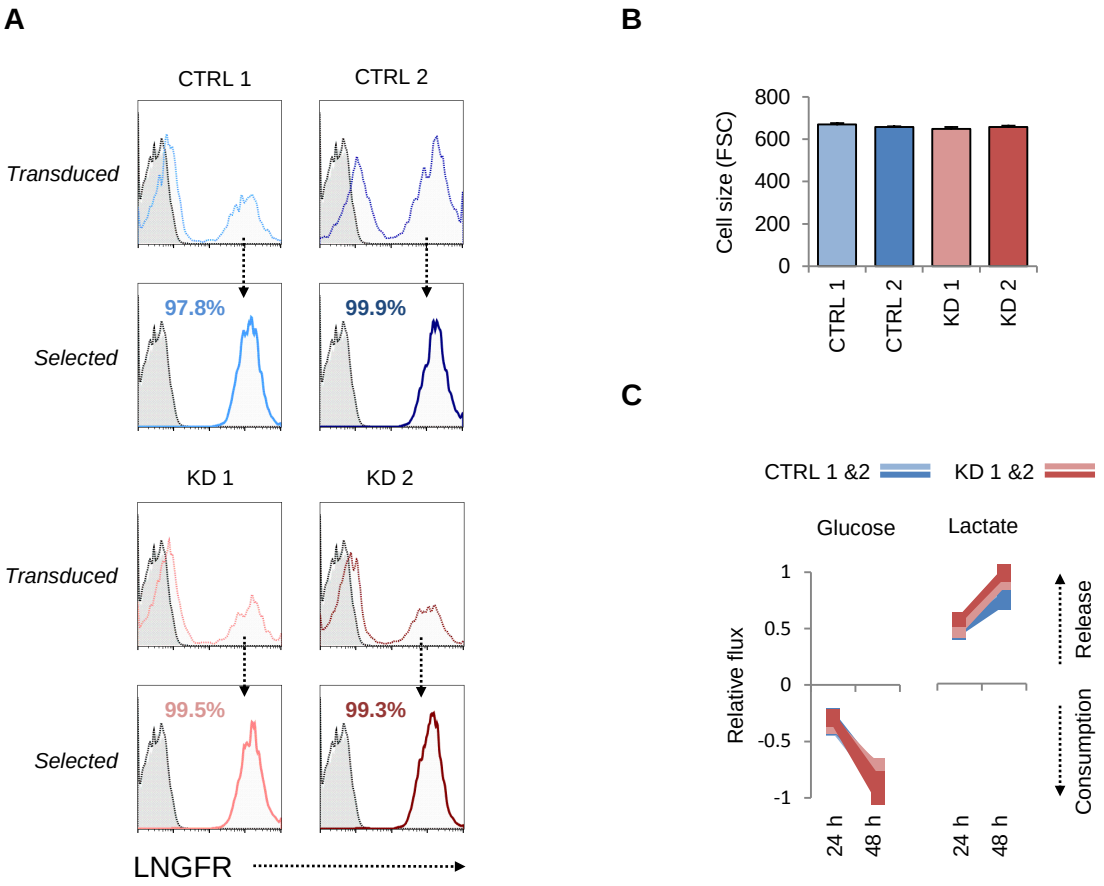

Figure S6. Controls for CoRe Metabolomics, Related to Figure 5

(A) Enrichment of transduced cells by AFMACS. Transduced cells from **Figures 5A-D** were stained with anti-LNGFR antibody before and after selection by AFMACS (red and blue lines). In each case, unstained cells (grey) and control cells stained with anti-LNGFR antibody (dotted line) are included and % LNGFR positive cells after selection are shown.

(B) No change in size of T-cells in response to SNAT1 depletion. Cells from **Figure 5B** were analysed by flow cytometry 48 hrs after re-stimulation with CD3/CD28 Dynabeads. Cell size is indicated by intensity of forward-scattered light (FSC). Mean values and 95% confidence intervals are shown for data obtained in triplicate.

(C) No change in glucose uptake or lactate release by SNAT1 depleted T-cells. As for **Figure 5D**, but net consumption or release of glucose and lactate by control and SNAT1-depleted cells is shown, scaled to a maximum change of 1.

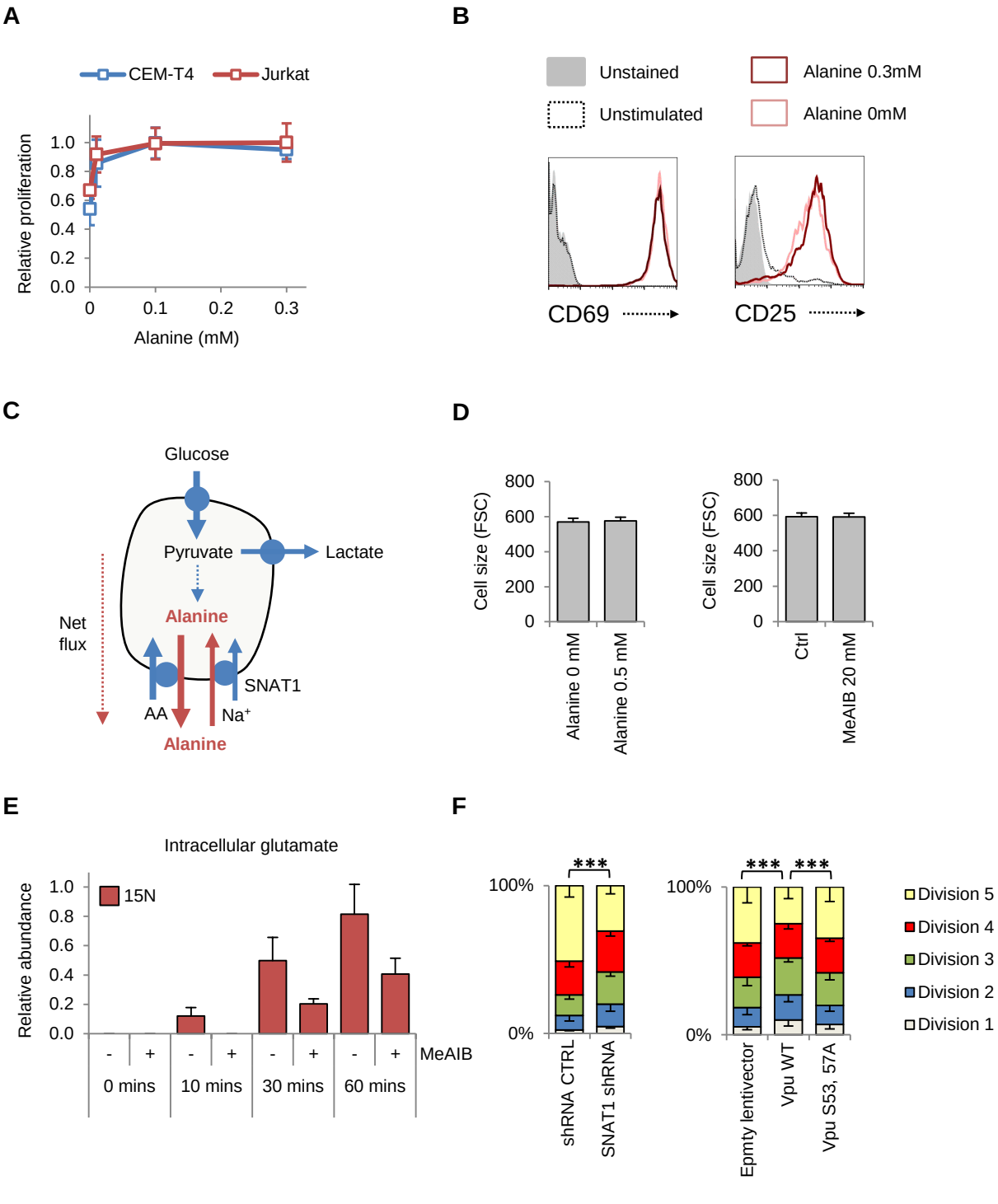

Figure S7. Controls for Free Intracellular Amino Acids, Related to Figure 6

(A) Dose-dependent proliferation of CEM-T4s and Jurkats in response to exogenous alanine. CEM-T4 and Jurkat T-cells were seeded in phenol red-free media supplemented with alanine at the concentrations indicated. Viable cells were enumerated using an MTT assay after 72 hrs and optical density expressed as fraction of maximum.

(B) Preserved CD69 and CD25 expression in the absence of alanine. As for **Figure 6A** but cells were stained with conjugated antibodies against CD69 and CD25 and analysed by flow cytometry after 24 hrs.

SUPPLEMENTAL TABLES

Please see supplied Excel spreadsheets for **Tables S1-3**.

Table S1. Interactive Spreadsheet of All TMT Timecourse Data, Related to Figure 1

Interactive spreadsheet enabling generation of temporal profiles of plasma membrane protein expression for any quantitated genes of interest ("Gene search and plots" worksheet). Instructions are included in the spreadsheet. The complete (unfiltered) TMT timecourse dataset from which plots are generated is included ("Complete TMT timecourse data" worksheet). Protein abundance is depicted on a colour scale (red = downregulated; green = upregulated). The number of unique peptides, peptides and peptide spectral matches are shown for each protein, along with ratio counts and variability for each TMT condition.

Table S2. Cluster #35 TMT and SILAC Timecourse Data, related to Figure 1

Spreadsheet of timecourse data for 134 proteins in Cluster #35 progressively downregulated by HIV infection. Protein abundance is depicted on a colour scale (red = downregulated; green = upregulated). As well as data from the TMT proteomic timecourse experiment, additional data from the SILAC proteomic validation timecourse experiment are also included. Not all proteins quantitated in the TMT experiment are seen in the SILAC experiment (this is typical for replicate proteomic experiments). The number of unique peptides is shown for each protein (TMT experiment) and each timepoint (SILAC experiment). Most confidence is attached to proteins identified by >1 unique peptide. Gene Ontology Cellular Component localisation information is shown for each protein: PM, plasma membrane; CS, cell surface; XC, extracellular; ShG, short GOCC (a subset of proteins with short membrane-specific GOCC terms but no subcellular assignment (Weekes et al., 2012); Mem, membrane. Where blank, no GOCC annotation is available.

Table S3. Functional Analysis of Proteins in Cluster #35, Related to Figure 2

Spreadsheet of DAVID functional annotation clusters enriched amongst proteins in Cluster #35 progressively downregulated by HIV infection, against a background of all quantitated proteins. Clusters with enrichment scores >1.3 (equivalent to a geometric means of all included enrichment p-values <0.05) are shown. Fold enrichment, unadjusted and Bonferroni-adjusted p-values for individual Gene Ontology Biological Process and Molecular Function terms are shown.

EXTENDED EXPERIMENTAL PROCEDURES

General Cell Culture

CEM-T4s (AIDS Reagent Program, Division of AIDS, NIAD, NIH: Dr J.P. Jacobs) (Foley et al., 1965) and Jurkats (Neil laboratory stocks) were cultured in RPMI supplemented with 10% FCS, 100units/ml penicillin and 0.1mg/ml streptomycin at 37°C in 5% CO_2. HEK 293Ts and HeLas (Lehner laboratory stocks) were cultured in DMEM supplemented with 10% FCS, 100units/ml penicillin and 0.1mg/ml streptomycin at 37°C in 5% CO_2. All cells were confirmed to be mycoplasma negative (Lonza MycoAlert).

Stable Isotope Labelling with Amino Acids in Cell Culture (SILAC)

For SILAC labelling, CEM-T4s were grown for at least 7 cell divisions in SILAC RPMI lacking lysine and arginine (Thermo Scientific) supplemented with 10% dialysed FCS (Gibco), 100units/ml penicillin and 0.1mg/ml streptomycin, 280mg/L proline (Sigma) and light (K0, R0; Sigma), medium (K4, R6; Cambridge Isotope Laboratories) or heavy (K8, R10; Cambridge Isotope Laboratories) $^{13}C/^{15}N$-containing lysine (K) and arginine (R) at 50mg/L.

Defined Culture Media

For experiments requiring stable isotope-labelled or defined concentrations of alanine plus/minus glucose, RPMI lacking amino acids and glucose (USBio) was supplemented with 10% dialysed FCS (Gibco), 50x RMPI amino acids, 10mM HEPES and alanine, glucose and glutamine at the concentrations indicated (all Sigma unless otherwise stated).

Primary Cell Isolation and Culture

Primary human CD4+ T cells were typically isolated from peripheral blood by density gradient centrifugation through Lympholyte-H (Cedarlane Laboratories) and negative selection using the Dynabeads Untouched Human CD4 T Cells kit (Invitrogen) according to the manufacturer's instructions. Purity was assessed by flow cytometry for CD3 and CD4 and routinely found to be ≥95%. Cells were cultured in RPMI supplemented with 10% FCS, 30U/ml recombinant human IL-2 (PeproTech), 100units/ml penicillin and 0.1mg/ml streptomycin at 37°C in 5% CO_2 and activated within 48hrs using Dynabeads Human T-Activator CD3/CD28 beads (CD3/CD28 Dynabeads; Invitrogen) according to the manufacturer's instructions.

For primary activation, cells were typically resuspended with CD3/CD28 Dynabeads at a density of 1-2x10^6 cells/ml in flat-bottomed plates or flasks with a 1:1 bead:cell ratio. Cell densities and culture areas were scaled in proportion. Cultures were expanded every 2-3

days using fresh media (including IL-2) and aiming to maintain cell density ≤2x10^6 cells/ml. For secondary activation, CD3/CD28 Dynabeads were removed after 7-10 days using a DynaMag-2 magnet (Invitrogen), and cells washed and resuspended in fresh media before re-stimulation according to the same protocol.

Ethics Statement

Ethical permission for this project was granted by the Cambridgeshire 2 Research Ethics Committee (REC reference 97/092). Informed written consent was obtained from all of the volunteers included in this study prior to providing blood samples.

HIV-1 Molecular Clones

pNL4-3-deltaE-EGFP (derived from the HIV-1 molecular clone pNL4-3 but encoding Enhanced Green Fluorescent Protein (EGFP) in the *env* open reading frame, rendering Env non-functional) was obtained through the AIDS Reagent Program, Division of AIDS, NIAD, NIH: Drs Haili Zhang, Yan Zhou, and Robert Siliciano (Zhang et al., 2004) and the complete sequence verified by Sanger sequencing (Source BioScience). To generate Vpu- and Nef-deficient viruses an XhoI-EcoRI restriction fragment was subcloned into pCDNA3(-)Pac and stop codons introduced early in the Vpu or Nef open reading frames by site-directed mutagenesis (based on the QuickChange system; Stratagene) using the following primers (mutagenized codons boxed):

Vpu forward: CATGTAATGCAACCTTGAATATAAGCAATAGTAGCATTAG

Vpu reverse: CTAATGCTACTATTGCTTATATTCAAGGTTGCATTACATG

Nef forward: CTATAAGATGGGTGGCAAGTAGTGATAAAGTAGTGTGATTGGATG

Nef reverse: CATCCAATCACACTACTTTATCACTACTTGCCACCCATCTTATAG

Restriction fragments were sub-cloned back into pNL4-3-deltaE-EGFP and mutations verified by Sanger sequencing (Source BioScience), immunoblot of infected CEM-T4s for Vpu and Nef proteins, and functional analysis of infected CEM-T4s by flow cytometry for EGFP, CD4 and tetherin.

In addition, the following HIV-1 molecular clones were utilised for particular experiments:

pNL4-3 – replication-competent virus (WT, ΔVpu, ΔNef, ΔVpuΔNef and Vpu phosphodegron and transmembrane mutants), used for infectious virus release assays and validation of SNAT1 downregulation in primary human CD4+ T-cells and 293Ts expressing SNAT1-HA

pNL4-3 Vpu 2_87 – Env-deficient virus (WT, ΔVpu, and Vpu phosphodegron mutant) encoding Vpu RP2v16_2_87 (Pickering et al., 2014) on a pNL4-3 background, used for T-cell proliferation assays

Vectors for Transgene Expression

For lentiviral transgene expression in CEM-T4s and HeLas, codon-optimised NL4-3 Vpu was sub-cloned from pCR3.1-Vpu-HA (Vigan and Neil, 2010) into pHRSIN-PGK-puro (van den Boomen et al., 2014) with (experiments in HeLas) or without (experiments in CEM-T4s) the C-terminal HA tag. Codon-optimised, untagged NL4-3 Nef (based on pNL4-3, Genbank: AF324493) was synthesised (GenScript) and subcloned into pHRSIN-PGK-puro.

For lentiviral expression in primary human CD4+ T cells, the same untagged, codon-optimised transgenes were subcloned into pHRSIN-SE-P2A-SBP-ΔLNGFR-W, encoding Vpu or Nef co-translated as Vpu/Nef-P2A-SBP-ΔLNGFR for Antibody-Free Magnetic Cell Sorting using the SBP-ΔLNGFR cell surface affinity tag (Matheson et al., 2014). To generate codon-optimised Vpu encoding S52A and S56A point mutations (Vpu S52, 56A) pCR3.1-Vpu-HA was subjected to site-directed mutagenesis (based on a modified version of the QuickChange system (Zheng et al., 2004)) using the following primers (mutagenized codons boxed):

Forward: AGGAC GCC GGCAACGAG GCC GAGGGCGAGGTGAGC

Reverse: CCCTC GGC CTCGTTGCC GGC GTCCTCGGCGCGCTC

Restriction fragments were sub-cloned into pHRSIN-SE-P2A-SBP-ΔLNGFR-W and mutations verified by Sanger sequencing (Source BioScience) and functional analysis of primary human CD4+ T cells transduced with Vpu- and Vpu S52, 56A-expressing lentiviruses using flow cytometry for LNGFR, CD4 and tetherin.

pCG-IRES-GFP vectors (mammalian expression vectors encoding Vpu or Nef variants as Vpu/Nef-IRES-GFP) have been previously described (Sauter et al., 2009). Sequence names identify HIV or SIV isolates from which Vpu variants are derived. Illustrative phylogenetic relationships were adapted from published phylogenetic trees based on Nef and Pol sequences (Kirchhoff, 2009; Schmokel et al., 2011; Sharp and Hahn, 2010; Takehisa et al., 2009). The SIVcpz lineage arose by recombination between SIVrcm and a common Vpu-encoding precursor of SIVgsn/mus/mon (SIVguenon). SIVden encodes a truncated Vpu protein and its phylogenetic relationship to the SIVgsn/mus/mon lineages is unclear (Dazza et al., 2005). HIV-1 and SIVgor viruses belong to a monophyletic cluster with SIVcpz viruses infecting the central *P. t. troglodytes* (*Ptt*) subspecies of chimpanzee (SIVcpz *Ptt*), with

SIVcpz viruses infecting the eastern *P. t. schweinfurthii* subspecies forming an outgroup (SIVcpz *Pts*). The control pCG-IRES-GFP vector (expressing GFP only) encodes a defective Nef with a mutation in the start codon and two premature stop codons (Sauter et al., 2009).

A SNAT1 cDNA clone was obtained from Open Biosystems in the pCMV-SPORT6 vector (IMAGE clone ID: 3871101; GenBank: BC010620.1; Entrez Gene ID: 81539 – *SLC38A1*). For lentiviral expression of full length C-terminally tagged SNAT1-FLAG, the following primer pairs were used for PCR amplification (FLAG sequence boxed):

Forward: GGATCCATCATGATGCATTTCAAAAGTGG

Reverse:
GGGCCCTCACTTATCGTCGTCATCCTTGTAATCTGCGGCCGCGTGGCCTTCGTCACTACTC

The resulting PCR products were ligated into pCR-Blunt-II TOPO, sequence-verified by Sanger sequencing (Source BioScience) and sub-cloned into pHRSIN-PGK-puro (van den Boomen et al., 2014) to generate pHRSIN-PGK-puro-SNAT1-FLAG.

For SNAT1 antibody production using GST-SNAT1 as an immunogen, the N-terminal 189 nucleotides of SNAT1 were amplified by PCR using the following primer pair:

Forward: GGATCCGCAGCTATGATGCATTTCAAAAGTGGAC

Reverse: GTCGACTCAACACTTCTTTTTTTCCAAATGGC

The resulting PCR product was ligated into pCR-Blunt II-TOPO, sequence verified by Sanger sequencing (Source BioScience) and sub-cloned into pGEX-4T-1 (a kind gift of Sally Gray) to create a single open reading frame encoding GST at the N-terminus fused with the N-terminal 63 amino acids of SNAT1 at the C-terminus (GST-SNAT1).

In addition, the following expression vectors were utilised for particular experiments:

pCR3.1 – mammalian expression vector encoding SERINC5, used for titration of HIV-1 infectious viral release

pCMS28 – pMigR1-based retroviral vector encoding Vpu-IRES-puro (Vpu WT, phosphodegron and transmembrane mutants), used for generation of stable Jurkat cell lines, or SNAT1-HA, used for generation of stable 293T cell lines expressing C-terminally tagged SNAT1-HA

pCSIG – pCS-based lentivector encoding Vpu RP2v16_2_87-IRES-GFP (Vpu WT, phosphodegron and transmembrane mutants), used for validation of SNAT1 downregulation in 293Ts expressing SNAT1-HA and T-cell proliferation assays

pQCXIH – pMSCV-based retroviral vector encoding human CD4-IRES-hygro (a kind gift from Professor Margaret Robinson), used for generation of stable 293T cell lines expressing CD4

Generation of the Vpu transmembrane mutants has been previously described (Vigan and Neil, 2010). As compared with NL4-3 Vpu phosphodegron (S52, 56A) and transmembrane (A14L, W22A) mutants, equivalent Vpu RP2v16_2_87 mutations are at residues S53, 57A and A15L, W23A, respectively.

Lentivectors for shRNA Expression

For lentiviral shRNA-mediated knockdown of SNAT1 in primary human CD4+ T cells, SNAT1-specific hairpins were cloned into pHRSIREN-S-SBP-ΔLNGFR-W (Matheson et al., 2014), encoding a U6-shRNA cassette and SFFV-SBP-ΔLNGFR for Antibody-Free Magnetic Cell Sorting using the SBP-ΔLNGFR cell surface affinity tag. Complementary shRNA-encoding oligonucleotides were designed using the Clontech on-line shRNA Sequence Designer, annealed, cloned into pHRSIREN using BamHI and EcoRI and sequence verified by Sanger sequencing (Source BioScience). The following (sense) targeting sequences were used:

SNAT1 shRNA KD 1: GGCAAACACTGGAATCCTA

SNAT1 shRNA KD 2: GATAGTTACCTTTGGCATA

SNAT1 shRNA KD 3: GAGAATCATGTGTACCTAA

Non-targeting control shRNA CTRL 1: GTTATAGGCTCGCAAAAGG

LacZ control shRNA CTRL 2: GTGACCAGCGAATACCTGT

The KD 1 sequence was selected using the Clontech on-line RNAi Target Sequence Selector. The KD 2 and KD 3 sequences were selected after deconvolution of a SNAT1-specific SMARTpool of four ON-TARGET*plus* siRNA oligonucleotides (Dharmacon). The CTRL 1 (control, scrambled) sequence (Matheson et al., 2014) and the CTRL 2 (control, targeting the bacterial *lacZ* gene) sequence (Qin et al., 2003) have been previously described. All sequences were searched against human RefSeq RNA using NCBI BLAST to confirm ≥4 mismatches with any contiguous off-target sequence.

KD 1 and CTRL 1 were used for all SNAT1 shRNA experiments except: KD 1, KD 2, CTRL 1 and CTRL 2 were used for Consumption and Release (CoRe) metabolomic analysis; and KD 3 and CTRL 1 were used for CellTrace Violet-based T-cell proliferation assays.

For generation of stable CEM-T4 cell lines, hairpins were cloned into pHRSIREN-PGK-puro, identical to pHRSIREN-S-SBP-ΔLNGFR-W but encoding PGK-puro for antibiotic selection (originally named pCSRQ and kindly provided by Professor Greg Towers) (Matheson et al., 2014; Schaller et al., 2011). For CellTrace Violet-based T-cell proliferation assays, hairpins were cloned into pHRSIREN-PGK-GFP, identical to pHRSIREN-S-SBP-ΔLNGFR-W and pHRSIREN-PGK-puro but encoding GFP for flow cytometric analysis.

siRNA Oligonucleotides

For transient siRNA-mediated knockdown of SNAT1, cells were transfected with a SNAT1-specific SMARTpool of four ON-TARGET*plus* siRNA oligonucleotides (Dharmacon). For β-TrCP and TSG101 knockdowns, siRNA oligonucleotides (Sigma) encoding the following (sense) targeting sequences were used:

β-TrCP siRNA: GTGGAATTTGTGGAACATC

TSG101 siRNA: CCUCCAGUCUUCUCUCGUC

The TSG101 sequence has been previously described (Hewitt et al., 2002). The β-TrCP sequence is fully conserved between β-TrCP1 and β-TrCP2 and effectively depletes both isoforms (Jin et al., 2003).

In all siRNA experiments, cells not subjected to knockdown were transfected with MISSION siRNA Universal Negative Control #2 (Sigma) at equivalent concentrations.

Transfections

FuGENE 6 (Promega; HIV-1 and lentivector production and general transfection), TransIT-293 (Mirus; general transfection) or polyethylenimine (Polysciences; HIV-1 and lentivector production) were used for plasmid DNA transfections in 293Ts. Oligofectamine (Invitrogen) was used for siRNA transfections in HeLas. siRNA oligonucleotides were used at a final concentration of 50nM and experiments were generally performed 48hrs after siRNA transfections. For TSG101 and β-TrCP knockdowns, a “two hit” approach was used, with an additional siRNA transfection after 24hrs (Hewitt et al., 2002).

Viral Stocks

VSVg-pseudotyped NL4-3-deltaE-EGFP HIV-1 viral stocks were generated by co-transfection of 293Ts with pNL4-3-deltaE-EGFP molecular clones and pMD.G at a ratio of 9:1 (µg) DNA and a DNA:FuGENE 6 ratio of 1µg:6µl. Media was changed the next day and viral supernatants harvested and filtered (0.45µm) at 48hrs prior to concentration with Lenti-X Concentrator (Clontech) and storage at -80°C.

VSVg-pseudotyped pHRSIN and pHRSIREN lentivector stocks were generated by co-transfection of 293Ts with lentivector, p8.91 and pMD.G at a ratio of 2:1:1 (µg) DNA and a DNA:FuGENE 6 ratio of 1ug:3µl. Viral supernatants were harvested, filtered, concentrated if required and stored as per NL4-3-deltaE-EGFP HIV-1 viral stocks.

VSVg-pseudotyped NL4-3 and NL4-3-Vpu 2_87 HIV-1 viral stocks were generated by co-transfection of 293Ts with pNL4-3 or pNL4-3-Vpu 2_87 molecular clones, respectively, and pCMV-VSV-G at a ratio of 5:1 (µg) DNA using polyethylenimine 1mg/ml (Polysciences). Media was changed the next day and viral supernatants harvested and filtered (0.45µm) at 48hrs then incubated at 37°C for 2hrs in the presence of 10µM $MgCl_2$ and 20U/ml DNAse (Roche) prior to concentration by ultracentrifugation through a 20% sucrose cushion and storage at -80°C.

VSVg-pseudotyped pCSIG lentivector stocks were generated by co-transfection of 293Ts with lentivector, pCRV1-HIV-1-Gag-Pol and pCMV-VSV-G at a ratio of 2:2:1 (µg) ratio using polyethylenimine 1mg/ml (Polysciences). Viral supernatants were harvested, filtered, DNAse-treated, concentrated and stored as per NL4-3 and NL4-3-Vpu 2_87 HIV-1 viral stocks.

VSVg-pseudotyped retroviral stocks were generated by co-transfection of 293Ts with pQCXIH or pCMS28 and plasmids encoding murine leukaemia virus (MLV) Gag-Pol and VSVg as previously described (Duncan et al., 2012; Randow, 2006).

Lentivector and NL4-3-deltaE-EGFP HIV-1 viral stocks were titred by infection/transduction of known numbers of relevant target cells under standard experimental conditions followed by flow cytometry at 48-72hrs to identify % infected/transduced cells. NL4-3 and NL43-Vpu 2_87 HIV-1 viral stocks were titred by infecting HeLa-TZM-bl indicator cells (AIDS Reagent Program, Division of AIDS, NIAD, NIH: Dr John C. Kappes) and counting focus-forming units by light microscopy following addition of X-Gal substrate at 48hrs.

All lentiviral and replication-competent HIV-1 viral work was performed under Biosafety Level 2 or 3 conditions, respectively.

Infections and Transductions

CEM-T4s were infected with concentrated HIV-1 viral stocks by spinoculation at 800g for 1-2hrs in a non-refrigerated benchtop centrifuge in complete media supplemented with 10mM HEPES. Primary human CD4+ T cells were transduced with concentrated HIV-1 or lentivector stocks using the same protocol 1 day after activation with CD3/CD28 Dynabeads. In experiments with reverse transcriptase inhibitors, cells were incubated with zidovudine (10uM) and efavirenz (100nM) (AIDS Reagent Program, Division of AIDS, NIAD, NIH) for 1hr prior to spinoculation, and inhibitors maintained at these concentrations during subsequent cell culture.

Stable Cell Lines

Stable CEM-T4 and HeLa cell lines were generated by transduction with pHRSIREN (control or SNAT1-specific shRNA expression) or pHRSIN (Vpu, Nef or GFP expression) lentivectors and selection with puromycin at 2µg/ml (CEM-T4) or 1µg/ml (HeLa). Stable Jurkat cell lines were generated by transduction with empty or Vpu-encoding pCMS28 retroviral vectors and selection with puromycin at 2µg/ml.

Stable SNAT1-FLAG and CD4-expressing 293T cell lines were generated by sequential transduction with pHRSIN-PGK-puro-SNAT1-FLAG and pQCXIH-CD4 and selection with puromycin at 1µg/ml and hygromycin at 200µg/ml. Transduced cells were screened by limiting dilution cloning and flow cytometry for high SNAT1-FLAG and CD4 cell surface expression. All experiments shown were conducted using clone S10.

Antibody-Free Magnetic Cell Sorting (AFMACS)

Antibody-Free Magnetic Cell Sorting of primary human CD4+ T cells using the streptavidin-binding SBP-ΔLNGFR affinity tag was carried out as previously described (Matheson et al., 2014). 3-5 days after primary activation and transduction with SBP-ΔLNGFR-encoding lentivectors, CD3/CD28 Dynabeads were removed using a DynaMag-2 magnet (Invitrogen). Cells were resuspended in Incubation Buffer (IB; PBS without calcium/magnesium, 2mM EDTA, 0.1% BSA) at 10^7 cells/ml and incubated with Dynabeads Biotin Binder (Invitrogen) at a bead-to-total cell ratio of 4:1 for 30mins at 4°C. Bead-bound cells expressing SBP-ΔLNGFR were selected using a DynaMag-2 magnet, washed to remove unbound non-transduced cells, then released from the beads by incubation in IB supplemented with 2mM biotin for 15mins at room temperature. Enrichment was assessed by flow cytometry for LNGFR pre- and post-selection. Cells were rested and then re-stimulated with CD3/CD28 Dynabeads 7-10 days after primary activation for use in downstream applications.

Tandem Mass Tag (TMT)-Based Plasma Membrane Profiling

Sample preparation

For the TMT-based HIV-1 infection timecourse, CEM-T4s were spinoculated with VSVg-pseudotyped NL4-3-deltaE-EGFP HIV-1 virus at a multiplicity of infection (MOI) of 10 in the presence or absence of reverse transcriptase inhibitors. Aliquots of cells were harvested sequentially, dead cells removed using the Miltenyi Dead Cell Removal kit, and plasma membrane enrichment carried out as previously described (Weekes et al., 2010; Weekes et al., 2012; Weekes et al., 2013; Weekes et al., 2014). All steps were performed on ice or at 4°C and washes were with ice-cold PBS with Ca/Mg pH 7.4 (Sigma) unless otherwise stated.

For aminooxy-biotinylation of plasma membrane proteins, $2x10^7$ viable cells per timepoint were washed and resuspended in a “one pot” aminooxy-biotinylation mix comprising 1mM sodium meta-periodate (Thermo Scientific), 100uM aminooxy-biotin (Biotium) and 10mM aniline (Sigma) in ice-cold PBS pH 6.7 and incubated for 30mins in the dark. After quenching with glycerol (1mM final concentration), cell pellets were washed and frozen at -80°C prior to downstream processing.

For affinity purification of aminooxy-biotinylated proteins, cell pellets were thawed on ice and lysed at 4°C for 30mins in TBS/1% Triton X-100 (high purity; Thermo Scientific) supplemented with Complete Protease Inhibitor Cocktail (without EDTA; Roche), 5mM iodoacetamide (Sigma) and 0.1mg/mL PMSF (Sigma). Nuclei and cell debris were removed by centrifugation and aminooxy-biotinylated plasma membrane proteins precipitated by incubation with High Capacity Streptavidin Agarose Resin (beaded agarose support; Thermo Scientific) at 4°C for at least 2hrs. Beads were transferred to Snap Cap spin columns (Thermo Scientific), reduced (100mM DTT) and alkylated (50mM iodoacetamide) at room temperature, and washed extensively using a vacuum manifold with (in total) >20 column volumes of TBS/1% Triton X-100 lysis buffer, PBS/0.5% SDS, TBS/6M urea, and, finally, H_2O. Beads were then transferred to small volume Screw Cap columns (Thermo Scientific) and incubated with 5ng/µl modified sequencing grade trypsin (Promega) in 100mM HEPES pH 8.5 at 37° for 6hrs. After digestion, peptide eluates were collected by centrifugation and stored at +4° prior to TMT labelling the next day.

For TMT labelling, Tandem Mass Tag 6-plex reagents (Thermo Scientific) were dissolved in anhydrous acetonitrile (0.8mg/40µl) and 10µl added to each peptide sample at a final acetonitrile concentration of 30% (v/v). Samples were labelled as follows: uninfected cells, 0hrs (TMT 126); 6hrs (TMT 127); 24hrs (TMT 128); 48hrs (TMT 129); 72hrs (TMT 130);

72hrs plus reverse transcriptase inhibitors (TMT 130). Following incubation at room temperature for 1 hr, reactions were quenched with hydroxylamine to a final concentration of 0.3% (v/v). Samples were mixed at a ratio of 1:1:1:1:1:1 and dried down to remove acetonitrile prior to off-line peptide fractionation.

Off-line High pH Reversed-Phase (HpRP) peptide fractionation

Tryptic peptides were subjected to HpRP-HPLC fractionation using a Dionex Ultimate 3000 powered by an ICS-3000 SP pump with an Agilent ZORBAX Extend-C18 column (4.6mm × 250mm, 5µm particle size). Mobile phases (H_20, 0.1% $NH_4{\circ}H$ or MeCN, 0.1% $NH_4{\circ}H$) were adjusted to pH 10.5 with the addition of formic acid and peptides were resolved using a linear 40min 0.1-40% MeCN gradient over 40mins at a 400µl/min flow rate and a column temperature of 15°C. Eluting peptides were collected in 15 s fractions. One hundred and twenty fractions covering the peptide-rich region were re-combined to give 10 samples for analysis. To preserve orthogonality, fractions were combined across the gradient, with each of the concatenated samples comprising 12 fractions which were 10 fractions apart. Re-combined fractions were dried down using an Eppendorf Concentrator and resuspended in 15µl MS solvent (3% MeCN, 0.1% TFA)

Mass spectrometry

Data for TMT labelled samples were generated using an Orbitrap Fusion Tribrid mass spectrometer (Thermo Scientific). Peptides were fractionated using an RSLCnano 3000 (Thermo Scientific) with solvent A comprising 0.1% formic acid and solvent B comprising 80% MeCN, 20% H_20, 0.1% formic acid. Peptides were loaded onto a 50cm Acclaim PepMap C18 column (Thermo Scientific) and eluted using a gradient rising from 10 to 25% solvent B by 90mins and 40% solvent B by 115mins at a flow rate of 250nl/min. MS data was acquired in the Orbitrap at 120,000fwhm between 400-1600 m/z. Spectra were acquired in profile with AGC 4.0e5. Ions with a charge state between 2+ and 6+ were isolated for fragmentation in top speed mode using the quadrupole with a 1.5 m/z isolation window. CID fragmentation was performed at 35% collision energy with fragments detected in the ion trap between 400-1200 m/z. AGC was set to 5.0e3 and MS2 spectra were acquired in centroid mode. TMT reporter ions were isolated for quantitation in MS3 using synchronous precursor selection. Ten fragment ions were selected for MS3 using HCD at 53% collision energy. Fragments were scanned in the Orbitrap at 60,000fwhm between 100-500 m/z with AGC set to 2.0e5. MS3 spectra were acquired in profile mode with injection parallelisation enabled.

Data processing and analysis

Raw MS files were processed using Proteome Discoverer 1.4.0.288 (Thermo Scientific). Data were searched against a concatenated human (UniProt, downloaded on 04/11/13) and HIV-1 (based on pNL4-3, Genbank: AF324493.2) database. VSVg (UniProt: P03522) and dEnv-EGFP-KDEL (inferred from the pNL4-3-deltaE-EGFP sequence) were substituted for Env. Precursor mass tolerance and fragment mass tolerance were set to 10ppm and 0.6Da, respectively, with a maximum of 2 missed tryptic cleavage sites. Percolator was used for post-processing of search results with a peptide false discovery rate of 0.01. Observed reporter ion intensities were adjusted for lot-specific isotopic impurities and missing quan values replaced with the minimum detected ion intensity. Protein abundances were calculated using unique peptides and normalised according to median protein ratios.

Gene Ontology Cellular Compartment (GOCC) terms were imported using Perseus 1.4.1.3 (downloaded from http://maxquant.org). To estimate the number of plasma membrane proteins quantitated, we counted proteins with GOCC terms “plasma membrane”, “cell surface” and “extracellular” or with short, membrane-specific GOCC terms but no subcellular assignment (Weekes et al., 2010; Weekes et al., 2012; Weekes et al., 2013; Weekes et al., 2014). Proteins with no GOCC terms were excluded from the denominator.

For clustering according to profiles of temporal expression, proteins identified by >1 unique peptide and with a minimum fold change from 0 of >2 were analysed using the Short Time Series Expression Miner (STEM) 1.3.8 (downloaded from www.cs.cmu.edu/Xjernst/stem) with default settings (Ernst and Bar-Joseph, 2006; Ernst et al., 2005). Significantly enriched temporal profiles were identified using a permutation-based test as previously described (Ernst et al., 2005). Unadjusted p-values are shown, but the number of genes assigned to a particular profile was only considered significant it the Bonferroni-corrected p-value was <0.05.

For functional analysis of proteins in Cluster #35, enrichment of Gene Ontology Biological Process and Molecular Function terms against a background of all proteins quantitated was determined using the Database for Annotation, Visualization and Integrated Discovery (DAVID) 6.7 (accessed on 5/8/14 at http://david.abcc.ncifcrf.gov) with default settings (Huang da et al., 2009a, b). Annotation clusters with enrichment scores >1.3 (equivalent to a geometric means of all included enrichment p-values <0.05) and terms with Bonferroni-adjusted p-values (EASE scores) <0.05 were considered significant.

For the interactive spreadsheet of all TMT data, gene name aliases were added using GeneALaCart (accessed on 27/5/15 at https://genealacart.genecards.org) (Rebhan et al., 1997).

The complete HIV-1 infection timecourse mass spectrometry proteomics dataset has been deposited to the ProteomeXchange Consortium (Vizcaino et al., 2014) via the PRIDE Proteomics Identifications (Vizcaino et al., 2013) partner repository with the dataset identifier PXD002934 (accessible at http://proteomecentral.proteomexchange.org).

SIALC-Based Plasma Membrane Profiling

Sample preparation

For the SILAC-based HIV-1 infection timecourse, CEM-T4s pre-labelled with heavy lysine and arginine were spinoculated with VSVg-pseudotyped NL4-3-deltaE-EGFP HIV-1 virus at an MOI of 10, and cells pre-labelled with medium lysine and arginine were mock spinoculated without virus. Aliquots of HIV-infected (heavy) and mock (medium) cells were harvested sequentially at the indicated timepoints, dead cells removed using the Miltenyi Dead Cell Removal kit, and equal cell numbers mixed prior to plasma membrane enrichment as described below.

For the SILAC-based analysis of Vpu and Nef deletion virus infections, CEM-T4s pre-labelled with heavy lysine and arginine were spinoculated with VSVg-pseudotyped Nef-deficient NL4-3-deltaE-EGFP HIV-1 virus at an MOI of 10, cells pre-labelled with medium lysine and arginine were spinoculated with VSVg-pseudotyped Vpu-deficient NL4-3-deltaE-EGFP HIV-1 virus at an MOI of 10, and cells pre-labelled with light lysine and arginine were retained as uninfected controls. HIV-infected (heavy and medium) and control (light) cells were harvested 72hrs after infection, dead cells removed using the Miltenyi Dead Cell Removal kit, and equal numbers mixed prior to plasma membrane enrichment as described below.

For the SILAC-based analysis of Vpu and Nef single gene over-expression, CEM-T4s transduced with GFP were labelled with light lysine and arginine, cells transduced with Vpu were labelled with medium lysine and arginine, and cells transduced with Nef were labelled with heavy lysine and arginine. Dead cells were removed using the Miltenyi Dead Cell Removal kit, and equal numbers mixed prior to plasma membrane enrichment as described below.

Plasma membrane enrichment and off-line peptide fractionation were carried out as for the TMT-based HIV-1 infection timecourse, except that proteins were digested in Protein LoBind

microcentrifuge tubes (Eppendorf) with 10ng/µl modified sequencing grade trypsin (Promega) in 50mM ammonium bicarbonate at 37° overnight, and peptide eluates were not subjected to TMT labelling.

Mass spectrometry

Data for SILAC labelled samples were generated on a Q Exactive orbitrap mass spectrometer (Thermo Scientific). Peptides were fractionated using an RSLCnano 3000 (Thermo Scientific) with solvent A comprising 0.1% formic acid and solvent B comprising 80% MeCN, 20% H_20, 0.1% formic acid. Peptides were loaded onto a 50cm C18 EASYspray column (Thermo Scientific) and eluted using a gradient rising from 10% to 36% B by 75mins and 55% B by 100mins. MS data was acquired at 70,000fwhm between 400-1650 m/z with AGC of 1e6 and 250ms injection time. MS2 data was acquired at 17,500fwhm with AGC of 5e4, 200ms injection time and a loop count of 10. HCD fragmentation was performed at NCE of 28% and an underfill ratio of 20%.

Data processing and analysis

Raw MS files were processed using MaxQuant 1.3.0.5. Data were searched against a concatenated human (UniProt, downloaded 04/11/13) and HIV-1 (based on pNL4-3, Genbank: AF324493.2) database. VSVg (UniProt: P03522) and dEnv-EGFP-KDEL (inferred from the pNL4-3-deltaE-EGFP sequence) were substituted for Env. Fragment ion tolerance was set to 0.5Da with a maximum of 2 missed tryptic cleavage sites. Carbamidomethyl (C) was defined as a fixed modification, oxidation (M), acetylation (protein N-terminal) and deamidation (NQ) were selected as variable modifications. A reversed decoy database was used with the false discovery rate for both peptides and proteins set at 0.01. Peptide re-quantify was enabled and quantitation utilized razor and unique peptides. Normalized protein ratios are reported.

For comparisons of protein expression across TMT and SILAC experiments, datasets were combined according to UniProt accession numbers using Perseus 1.4.1.3. For validation of Cluster #35 downregulation in the SILAC-based HIV-1 infection timecourse, expression ratios of proteins in Cluster #35 were compared with expression ratios of all other proteins at each timepoint using 2-tailed 2-sample T-tests (assuming homoscedasticity) conducted using Excel.

Consumption and Release (CoRe) Metabolomics

Sample preparation

Primary human CD4+ T cells were activated with CD3/CD28 Dynabeads and transduced with pHRSIREN-S-SBP-ΔLNGFR-W lentivectors encoding control or SNAT1-specific shRNAs. Transduced cells were selected using Antibody-Free Magnetic Cells Sorting, rested and then re-stimulated using CD3/CD28 Dynabeads. After a further 24hrs, cells were resuspended at $5x10^5$ cells/ml in 20% conditioned media plus 10mM HEPES and supernatant samples obtained at baseline, 24 and 48hrs. For calculation of metabolite consumption/release, cell-free media samples were obtained at matched timepoints. Supernatants and media samples were stored at -80°C prior to analysis by mass spectrometry. The experiment was conducted in triplicate and cells enumerated at each timepoint using Dako CytoCount beads.

Metabolite profiling

Polar metabolites in media were profiled in both positive and negative ionization modes using two liquid chromatography tandem mass spectrometry (LC-MS) methods as described previously (Townsend et al., 2013). The methods were developed using authentic reference standards for each metabolite to determine chromatographic retention times and multiple reaction monitoring MS parameters, including declustering potentials and collision energies. Briefly, negative ionization mode data were acquired using an ACQUITY UPLC (Waters) coupled to a 5500 QTRAP triple quadrupole mass spectrometer (AB SCIEX). Media samples (30µL) were extracted using 120µl of 80% methanol containing 0.05ng/µl inosine-15N4, 0.05ng/µL thymine-d4, and 0.1ng/µl glycocholate-d4 as internal standards (Cambridge Isotope Laboratories). The samples were centrifuged (10mins, 9,000g, 4ºC) and the supernatants (10µl) were injected directly onto a 150mm x 2.0mm Luna NH2 column (Phenomenex, Torrance CA). The column was eluted at a flow rate of 400µl/min with initial conditions of 10% mobile phase A (20mM ammonium acetate and 20mM ammonium hydroxide (Sigma) in water (VWR)) and 90% mobile phase B (10mM ammonium hydroxide in 75:25 v/v acetonitrile/methanol (VWR)) followed by a 10min linear gradient to 100% mobile phase A. The ion spray voltage was -4.5kV and the source temperature was 500°C.

Positive ionization mode data were acquired using a 4000 QTRAP triple quadrupole mass spectrometer (AB SCIEX) coupled to a 1200 Series binary HPLC pump (Agilent) and an HTS PAL autosampler (Leap Technologies). Media samples (10µL) were extracted using nine volumes of 74.9:24.9:0.2 (v/v/v) acetonitrile/methanol/formic acid containing stable isotope-labelled internal standards (0.2ng/µl valine-d8, Isotec; and 0.2ng/µL phenylalanine-

d8 (Cambridge Isotope Laboratories)). The samples were centrifuged (10mins, 9,000g, 4ºC) and the supernatants (10µl) were injected onto a 150 x 2.1mm Atlantis HILIC column (Waters). The column was eluted isocratically at a flow rate of 250µl/min with 5% mobile phase A (10mM ammonium formate and 0.1% formic acid in water) for 1min followed by a linear gradient to 40% mobile phase B (acetonitrile with 0.1% formic acid) over 10mins. The ion spray voltage was 4.5kV and the source temperature was 450°C. Raw data were processed using MultiQuant 1.2 software (AB SCIEX) for automated peak integration. Metabolite peaks were manually reviewed for quality of integration and compared against reference standards to confirm identities.

Data analysis

For each supernatant sample, measured metabolite peak areas at 24 or 48hrs (S_{24} or S_{48}) were converted to per-cell consumption/release data ($CoRe_{24}$ or $CoRe_{48}$) by subtracting peak areas from cell-free media harvested at the same timepoint (M_{24} or M_{48}) and normalising according to average cell numbers. Changes in media volume over the 48 hr period were negligible. Cells numbers at baseline, 24 and 48hrs (n_0, n_{24} and n_{48}) were used to calculate average cell numbers from 0-24 and 0-48hrs as $(n_0 + n_{24})/2$ and $(n_0 + 2*n_{24} + n_{48})/4$, respectively. Therefore, for each metabolite: $CoRe_{24} = 2*(S_{24} - M_{24})/(n_0 + n_{24})$ and $CoRe_{48} = 4*(S_{48} - M_{48})/(n_0 + 2*n_{24} + n_{48})$. Metabolites with missing values were censored.

For multivariate comparison of metabolite profiles from control and SNAT1-depleted cells at 24 and 48hrs, CoRe data were autoscaled prior to Principal Component Analysis using MetaboAnalyst software (accessed at www.metaboanalyst.ca) (Xia et al., 2012; Xia et al., 2009; Xia et al., 2015). For univariate analysis of consumption/release of individual metabolites from control and SNAT1-depleted cells at 48hrs, 2-tailed 2-sample T-tests (assuming homoscedasticity) were conducted using Excel, with p-values corrected by the Bonferroni method. For graphical representation of individual metabolite consumption/release, CoRe data were scaled so that the maximum absolute value for each metabolite was equal to 1 (Jain et al., 2012).

3H-Alanine Uptake

3H-Alanine uptake was measured using an optimised method of silicone oil filtering centrifugation (Carr et al., 2010; Edinger and Thompson, 2002; Iiboshi et al., 1999; Pozueta-Romero et al., 1991; Werkheiser and Bartley, 1957). Primary human CD4+ T cells were activated with CD3/CD28 Dynabeads and transduced with pHRSIREN-S-SBP-ΔLNGFR-W or pHRSIN-SE-P2A-SBP-ΔLNGFR-W lentivectors encoding control or SNAT1-specific shRNAs, or Vpu or Vpu S52, 56A, respectively. Transduced cells were selected using

Antibody-Free Magnetic Cells Sorting, rested and then re-stimulated using CD3/CD28 Dynabeads. After a further 48-72hrs CD3/CD28 Dynabeads were removed using a DynaMag-2 magnet (Invitrogen) and cells enumerated using Dako CytoCount beads. Washed cells were then equilibrated in HBSS/2% dialysed FCS (Gibco) at $1x10^6$ cells/ml for 30-60mins at 37°C to deplete intracellular amino acids and reduce trans-inhibition (Iruloh et al., 2009; Iruloh et al., 2007). Starved cells were resuspended in Tyrode's buffer (NaCl 135mM, KCl 5mM, $CaCl_2$ 1.8mM, $MgCl_2$ 1mM, HEPES 10mM, glucose 5.6mM)/2% dialysed FCS at 2 $x10^6$ cells/ml and uptake at 37° initiated by addition of 3H-alanine (PerkinElmer) to a final concentration of 0.5mM (1µCi/timepoint). Aliquots of cells were harvested sequentially over 5mins. Each aliquot was transferred to the centre of the top layer of a pre-cooled 0.4ml microcentrifuge tube (Alpha Laboratories) containing: top layer 125µl PBS; middle layer 125µl silicone oil AR20/AR200 = 3/1 (Sigma); bottom layer 50µl 10% sucrose/H_2O). Tubes were spun immediately at 13,000g for 1min at 4°C, top and middle layers carefully aspirated using an extended length pipette tip (STARLAB) and cell pellets lysed for at least 30mins at 4°C by addition of 50µl 2% Triton/PBS. Lysates were combined with 4ml Ultima Gold MV (PerkinElmer) in Liquid Scintillation Counting vials (PerkinElmer) and counted on an LS 6500 scintillation counter (Beckman). Where specified, System A amino acid transport was inhibited with methylaminoisobutyric acid (MeAIB, 20mM; Abcam) (Mackenzie and Erickson, 2004; Tsitsiou et al., 2009). Control measurements with no cells routinely produced counts identical to background, suggesting highly efficient separation of cells from uptake buffer. Under the conditions used, 3H-Alanine uptake was found to be linear (corresponding to initial rate), Na-dependent and saturable with unlabelled alanine. Counts per minute (CPM) were plotted against time and linear regression lines with 95% confidence bands added using XLSTAT. Slopes (indicating rates of uptake) were compared using 2-tailed T-tests (assuming homoscedasticity) conducted using Excel.

Free Intracellular Amino Acids and Stable Isotopologue-Resolved Metabolomics

Sample preparation

Primary human CD4+ T-cells were expanded with CD3/CD28 Dynabeads, rested for 7-10 days, then re-stimulated using CD3/CD28 Dynabeads. After a further 48hrs CD3/CD28 Dynabeads were removed using a DynaMag-2 magnet (Invitrogen) and cells enumerated using Dako CytoCount beads. Washed cells were then resuspended at 37°C in RPMI supplemented with 10% dialysed FCS, glucose (5.6mM), glutamine (0.5mM) and alanine (concentrations as indicated). For stable isotope tracing, 13C6-glucose and 15N-alanine (both Cambridge Isotope Laboratories) were used. Where specified, System A amino acid transport was inhibited with methylaminoisobutyric acid (MeAIB, 20mM; Abcam) (Mackenzie

and Erickson, 2004; Tsitsiou et al., 2009). Aliquots of cells were harvested at the indicated timepoints, washed with ice-cold PBS, and snap frozen on dry ice. Free intracellular amino acids were extracted using dry ice-cold 50% methanol 30% acetonitrile and stored at -80°C prior to analysis by mass spectrometry. Cell size was determined by flow cytometry.

Mass spectrometry

LC-MS analysis was performed on a Q Exactive orbitrap mass spectrometer coupled to an Accela LC system (Thermo Scientific). The liquid chromatography system was fitted with either a Sequant Zic-HILIC column (column A, 150mm × 4.6mm, i.d. 3.5µm), or a Sequant Zic-pHilic (column B, 150mm × 2.1mm, i.d. 3.5µm) with guard columns (20mm × 2.1mm, i.d. 3.5µm) from HiChrom, Reading, UK. With column A, the mobile phase was composed by 0.1% aqueous formic acid (solvent A) and 0.1% formic acid in acetonitrile (solvent B). The flow rate was set at 300µl/min and the gradient was as follows: 0-3mins 80% B, 25mins 20% B, 26mins 80 % B, 36mins 80% B. For column B, the mobile phase was composed of 20mM ammonium carbonate and 0.1% ammonium hydroxide in water (solvent C), and acetonitrile (solvent D). The flow rate was set at 180µl/min with the following gradient: 0min 80% D, 28mins 20% D, 29mins 80% D, 45mins 80% D. The mass spectrometer was operated in full MS and polarity switching mode. Samples were randomised in order to avoid machine drifts. The acquired spectra were analysed using XCalibur Qual Browser and XCalibur Quan Browser softwares (Thermo Scientific). Mean metabolite abundance is expressed as fraction of maximum, with 95% confidence intervals shown for data obtained in triplicate.

SNAT1 Antibodies

Anti-SNAT1 (H60) rabbit polyclonal antibody (Santa Cruz Biotechnology) was used for Western blot and re-immunoprecipitation. Anti-SNAT1 (G63) rabbit polyclonal antibody (made in-house) was used for immunofluorescence microscopy and immunoprecipitation. To generate anti-SNAT1 (G63), glutathione S-transferase (GST)-SNAT1 fusion protein (incorporating the N-terminal 63 amino acids of SNAT1) was expressed in *E. coli* and purified from bacterial lysate by affinity chromatography using immobilised glutathione according to standard methods (GE, 2010). Unfused GST protein was also expressed and purified using empty pGEX-4T-1 vector. Fusion protein was detectable by immunoblotting with anti-SNAT1 (H60) and confirmed to run at approximately 33kDa by SDS-PAGE (compared with GST at approximately 26kDa) with no significant contaminating bands visualised by Coomassie staining. GST-SNAT1 was used to immunize 2 rabbits (Cambridge Research Biochemicals) and, after screening of crude sera by Western blot, serum from rabbit #5297 was selected for affinity purification. Serum was pre-sorbed against immobilised GST (to remove GST-specific antibodies) then purified by affinity

chromatography against immobilised GST-SNAT1 using the Pierce GST Orientation kit (Thermo Scientific) according to the manufacturer's instructions. Affinity-purified antibody was validated for detection of SNAT1 by immunofluorescence microscopy and immunoprecipitation using 293Ts over-expressing SNAT1 or depleted of SNAT1 by RNAi and CEM-T4s and primary human CD4+ T cells depleted of SNAT1 by RNAi. Aliquots were stored at -20°C in PBS/1% BSA/0.02% azide.

Other Antibodies

The following primary antibodies were used for flow cytometry (alphabetical order): anti-CD4-Brilliant Violet (clone OKT4; BioLegend); anti-CD4-Pacific Blue and anti-CD4-PE (clone RPA-T4; BD Biosciences); anti-CD25-PE (clone M-A251; BD Biosciences); anti-CD43-APC (clone CD43-10G7; BioLegend); anti-CD47-PerCP (clone CC2C6; BioLegend); anti-CD50 (clone TU41; BD Biosciences); anti-CD69-APC (clone FN50; BioLegend); anti-CD162-PE (clone KPL-1; BioLegend); anti-FLAG (rabbit polyclonal; Sigma); anti-LNGFR-APC and anti-LNGFR-PE (clone ME20.4; BioLegend); anti-NOTCH1-APC (clone MHN1-519; eBioscience); anti-p24-RD1 (clone KC57; Beckman Coulter); anti-tetherin (clone 3H4; Abnova) and anti-tetherin-APC (clone RS38E; BioLegend). As a functional assay for NCR3LG1 expression, recombinant human NKp30-Ig chimera (R&D Systems) was used in place of a primary antibody.

The following primary antibodies were used for immunoblots (alphabetical order): anti-α-tubulin (clone DM1A; Sigma); anti-ß-actin (clone AC-74; Sigma); anti-ß-TrCP (rabbit polyclonal H-300; Santa Cruz Biotechnology); anti-HA (clone HA.11/16B12; Covance); anti-HSP90 (rabbit polyclonal; Santa Cruz Biotechnology); anti-ubiquitin (clone VU-1; LifeSensors); anti-TSG101 (clone 4A10; GeneTex). Anti-Vpu and anti-p24 were obtained through the NIH AIDS Reagent Program, Division of AIDS, NIAID, NIH: Dr Klaus Strebel and Dr Bruce Chesebro, respectively (Maldarelli et al., 1993).

The following secondary antibodies were used: goat anti-mouse-AF647 and anti-rabbit-AF647 (flow cytometry; Molecular Probes); donkey anti-human-PE (flow cytometry; Jackson ImmunoResearch); goat anti-mouse-HRP and anti-rabbit-HRP (immunoblot, Jackson ImmunoResearch); donkey anti-goat-AF488 (immunofluorescence microscopy; Molecular Probes).

Flow Cytometry

Where necessary, CD3/CD28 Dynabeads were removed from primary human CD4+ T cells using a DynaMag-2 magnet (Invitrogen) prior to analysis. Typically $2x10^5$ washed cells were incubated for 30mins in 100µl PBS with the indicated fluorochrome-conjugated antibody or stained sequentially with primary and fluorochrome-conjugated secondary antibodies. All steps were performed on ice or at 4°C and stained cells were analysed immediately or fixed in PBS/1% paraformaldehyde. For NKp30-Ig staining, cells were first blocked for 30mins in PBS supplemented with 10% donkey serum (Sigma). For p24 staining, cells were first fixed and permeabilised using the BD Cytofix/Cytoperm method (BD Biosciences). Viability was assessed using forward and side scatter or, for CellTrace Violet-based T-cell proliferation assays, using the LIVE/DEAD Fixable Near-IR Dead Cell Stain kit (Molecular Probes). Where indicated, absolute cell numbers were determined using CytoCount beads (Dako) as a reference population. Cells were analysed using a BD FACSCalibur, FACSCanto II, LSRFortessa or ADP Cyan flow cytometer, and data processed using FlowJo software. For comparisons of fluorescence intensity, geomean fluorescence was used. For comparisons of cell size, mean intensity of forward-scattered light (FSC) was used.

Immunoblotting

Cells were typically lysed in TBS/1% Triton X-100 or PBS/1% SDS supplemented with 0.5mM phenylmethylsulfonyl fluoride (PMSF), 5mM iodoacetamide (IAA) and Complete Protease Inhibitor Cocktail (Roche) for 30mins on ice or at room temperature, respectively. For SDS lysis, Benzonase (Sigma) was included to reduce lysate viscosity. Post-nuclear supernatants were heated in Laemelli Loading Buffer for 25mins at 50°C, separated by SDS-PAGE and transferred to Immobilon-P membrane (Millipore). Membranes were blocked in PBS/5% non-fat dried milk (Marvel)/0.2% Tween and probed with the indicated primary antibody overnight at 4°C. Reactive bands were visualised using HRP-conjugated secondary antibodies and SuperSignal West Pico or Dura chemiluminescent substrates (Thermo Scientific). 8% Tris-glycine or 4-12% NuPAGE Bis-Tris gels were used to resolve SNAT1 and sample loading was by equivalent cell number (typically $1x10^5$/lane) or total protein (typically 10µg/lane; Pierce BCA Protein Assay kit; Thermo Scientific) depending on cell type. Where indicated, cells were pre-treated with MG132 (50µM for 4hrs; Cayman Chemical), lactacystin (20µM for 16hrs; Boston Biochem), concanamycin A (50nM for 16hrs; Calbiochem) or bafilomycin A1 (200nM for 16hrs; Calbiochem).

Immunoprecipitation

For co-immunoprecipitation of SNAT1 and Vpu-HA, 10^6 HeLas (transduced or transfected as indicated) were incubated with bafilomycin A (400nM for 4hrs; Calbiochem) prior to solubilisation in 1% Triton X-100. Lysates were pre-cleared with a combination of Protein A-Sepharose (Sigma) and IgG-Sepharose (GE Healthcare) and incubated for 1 hr at 4°C with anti-SNAT1 (G63)/Protein A-Sepharose (Sigma; for immunoprecipitation of SNAT1) or anti-HA coupled to agarose beads (Sigma EZview Red Anti-HA Affinity Gel; for immunoprecipitation of Vpu-HA). After washing in 1% Triton X-100, samples were eluted in SDS sample buffer, separated by SDS-PAGE, and immunoblotted as described.

For detection of ubiquitinated SNAT1, anti-SNAT1 (G63)-immunoprecipitated samples (as above) were washed in 1% Triton X-100 and denatured with 0.5% SDS before 50-fold dilution in 1% Triton X-100 and re-immunoprecipitation with anti-SNAT1 (H60). After further washing in 1% TritonX-100, samples were treated with Peptide-N-Glycosidase F (NEB) and separated by SDS-PAGE. Proteins were transferred to PVDF membranes and crosslinked with 0.5% glutaraldehyde/PBS for 20mins before probing with anti-ubiquitin (VU-1) and visualisation as described.

Immunofluorescence Microscopy

Where necessary, CD3/CD28 Dynabeads were removed from primary human CD4+ T cells using a DynaMag-2 magnet (Invitrogen) prior to analysis. Typically $2x10^5$ cells were seeded in serum-free media for 30mins on 13mm coverslips pre-coated with 100µg/ml poly-D-lysine (Sigma). Cells were fixed and permeabilised for 5mins on ice with 100% MeOH pre-cooled to -20°C then blocked for 1 hr at room temperature in PBS/1% BSA supplemented with 5% donkey serum (Sigma) and Vivaglobin (160mg/ml human normal immunoglobulin; CSL Behring) 1/1000. Cells were stained sequentially for 1 hr at room temperature with anti-SNAT1 (G63) and donkey anti-goat-AF488 (Molecular Probes) in PBS/1% BSA and washed with PBS/0.1% Tween-20. For confocal microscopy, coverslips were mounted using ProLong Gold Antifade Mountant with DAPI (Invitrogen) before analysis using a Zeiss LSM510 or LSM710 confocal microscope. For Total Internal Reflection (TIRF) microscopy, coverslips were stained with DAPI 1/2000 in PBS and fixed in PBS/1% PFA for 15mins at room temperature before analysis with a Zeiss TIRF3 microscope. Representative images are shown.

Cell Proliferation

For titration of exogenous alanine in CEM-T4s and Jurkats, cells were seeded in a 96-well plate format in phenol red-free RPMI supplemented with 10% dialysed FCS, glutamine (2mM) and alanine (range of concentrations 0-0.3mM as indicated). Viable cell numbers were determined after 72hrs using an MTT (Thiazolyl Blue Tetrazolium Bromide) assay as previously described (Twentyman and Luscombe, 1987). After incubation with MTT (Sigma) 1mg/ml for 4hrs at 37°C, media was aspirated, formazan crystals solubilised in DMSO and optical density measured at 540nm.

For titration of exogenous alanine in primary human CD4+ T-cells, cells were stained with carboxyfluorescein succinimidyl ester (CFSE) and proliferation analysed according to standard methods. CFSE (Molecular Probes) was resuspended in DMSO at 5mM and stored at -20°C. Freshly isolated T-cells were incubated in 5μM CFSE/PBS/0.5% dialysed FCS at 10^7 cells/ml for 5mins at room temperature with continuous overhead rotation. Staining was quenched with 5 volumes of ice-cold complete medium and cells incubated on ice for 5mins. Washed cells were then resuspended in RPMI supplemented with 10% dialysed FCS, glucose (5.6mM), glutamine (0.5mM) and alanine (range of concentrations 0-0.3mM as indicated) before activation with CD3/CD28 Dynabeads. Cells were expanded with fresh media (containing matched concentrations of alanine) at 48hrs and CFSE fluorescence measured by flow cytometry after a further 72hrs.

For proliferation of primary human CD4+ T-cells transduced with GFP-expressing lentivectors, CellTrace Violet (Molecular Probes) was substituted for CFSE. Cells were typically activated with CD3/CD28 Dynabeads, transduced after 24hrs, and analysed by flow cytometry after a further 96hrs. CellTrace Violet fluorescence was evaluated in viable, GFP+ (transduced) cells. The same method was used to assess proliferation of primary human CD4+ T-cells infected with HIV-1, but CellTrace Violet fluorescence was evaluated in viable, p24+ (infected) cells. Mean % cells in each generation were compared using two-way repeated measures ANOVA conducted using Prism 5 (GraphPad Software).

For competition between exogenous alanine and MeAIB in primary human CD4+ T-cells, cells were seeded in a 96-well plate format in RPMI supplemented with 10% dialysed FCS, glucose (10.2mM), glutamine (0.6mM), alanine (range of concentrations 0-0.3mM as indicated) and MeAIB (range of concentrations 0-20mM as indicated) before activation with CD3/CD28 Dynabeads. Absolute cell numbers were determined by flow cytometry after 72hrs, using CytoCount beads (Dako) as a reference population.

Infectious Viral Release

For titration of SERINC5, 293Ts cells were co-transfected in a 24-well plate format with 500ng pNL4-3 HIV-1 molecular clones plus indicated concentrations of pCR3.1-SERINC5 using polyethylenimine 1mg/ml (Polysciences) and pCR3.1-GFP as a bulking plasmid. Culture supernatants were harvested after 48hrs. Infectious viral release was determined by infecting HeLa-TZM-bl indicator cells (AIDS Reagent Program, Division of AIDS, NIAD, NIH: Dr John C. Kappes) and measuring chemiluminescent β-galactosidase activity after 48hrs using the Tropix Galacto-Star system (Applied Biosystems) as previously described (Vigan and Neil, 2010). For SNAT1-HA over-expression, control and SNAT1-HA-expressing 293Ts were infected with VSVg-pseudotyped NL4-3 HIV-1 viruses at an MOI of 2. Culture supernatants were harvested after 48hrs, and infectious viral release determined by the same method.

SUPPLEMENTAL REFERENCES

Carr, E.L., Kelman, A., Wu, G.S., Gopaul, R., Senkevitch, E., Aghvanyan, A., Turay, A.M., and Frauwirth, K.A. (2010). Glutamine uptake and metabolism are coordinately regulated by ERK/MAPK during T lymphocyte activation. J Immunol *185*, 1037-1044.

Dazza, M.C., Ekwalanga, M., Nende, M., Shamamba, K.B., Bitshi, P., Paraskevis, D., and Saragosti, S. (2005). Characterization of a novel vpu-harboring simian immunodeficiency virus from a Dent's Mona monkey (Cercopithecus mona denti). J Virol *79*, 8560-8571.

Drakesmith, H., Chen, N., Ledermann, H., Screaton, G., Townsend, A., and Xu, X.N. (2005). HIV-1 Nef down-regulates the hemochromatosis protein HFE, manipulating cellular iron homeostasis. Proc Natl Acad Sci U S A *102*, 11017-11022.

Duncan, L.M., Timms, R.T., Zavodszky, E., Cano, F., Dougan, G., Randow, F., and Lehner, P.J. (2012). Fluorescence-based phenotypic selection allows forward genetic screens in haploid human cells. PLoS One *7*, e39651.

Edinger, A.L., and Thompson, C.B. (2002). Akt maintains cell size and survival by increasing mTOR-dependent nutrient uptake. Mol Biol Cell *13*, 2276-2288.

Ernst, J., and Bar-Joseph, Z. (2006). STEM: a tool for the analysis of short time series gene expression data. BMC Bioinformatics *7*, 191.

Ernst, J., Nau, G.J., and Bar-Joseph, Z. (2005). Clustering short time series gene expression data. Bioinformatics *21 Suppl 1*, i159-168.

Foley, G.E., Lazarus, H., Farber, S., Uzman, B.G., Boone, B.A., and McCarthy, R.E. (1965). Continuous Culture of Human Lymphoblasts from Peripheral Blood of a Child with Acute Leukemia. Cancer *18*, 522-529.

GE (2010). GST Gene Fusion System Handbook.

Hewitt, E.W., Duncan, L., Mufti, D., Baker, J., Stevenson, P.G., and Lehner, P.J. (2002). Ubiquitylation of MHC class I by the K3 viral protein signals internalization and TSG101-dependent degradation. EMBO J *21*, 2418-2429.

Huang da, W., Sherman, B.T., and Lempicki, R.A. (2009a). Bioinformatics enrichment tools: paths toward the comprehensive functional analysis of large gene lists. Nucleic Acids Res *37*, 1-13.

Huang da, W., Sherman, B.T., and Lempicki, R.A. (2009b). Systematic and integrative analysis of large gene lists using DAVID bioinformatics resources. Nat Protoc *4*, 44-57.

Iiboshi, Y., Papst, P.J., Kawasome, H., Hosoi, H., Abraham, R.T., Houghton, P.J., and Terada, N. (1999). Amino acid-dependent control of p70(s6k). Involvement of tRNA aminoacylation in the regulation. J Biol Chem *274*, 1092-1099.

Iruloh, C.G., D'Souza, S.W., Fergusson, W.D., Baker, P.N., Sibley, C.P., and Glazier, J.D. (2009). Amino acid transport systems beta and A in fetal T lymphocytes in intrauterine growth restriction and with tumor necrosis factor-alpha treatment. Pediatr Res *65*, 51-56.

Iruloh, C.G., D'Souza, S.W., Speake, P.F., Crocker, I., Fergusson, W., Baker, P.N., Sibley, C.P., and Glazier, J.D. (2007). Taurine transporter in fetal T lymphocytes and platelets: differential expression and functional activity. Am J Physiol Cell Physiol *292*, C332-341.

Jain, M., Nilsson, R., Sharma, S., Madhusudhan, N., Kitami, T., Souza, A.L., Kafri, R., Kirschner, M.W., Clish, C.B., and Mootha, V.K. (2012). Metabolite profiling identifies a key role for glycine in rapid cancer cell proliferation. Science *336*, 1040-1044.

Jin, J., Shirogane, T., Xu, L., Nalepa, G., Qin, J., Elledge, S.J., and Harper, J.W. (2003). SCFbeta-TRCP links Chk1 signaling to degradation of the Cdc25A protein phosphatase. Genes Dev *17*, 3062-3074.

Kirchhoff, F. (2009). Is the high virulence of HIV-1 an unfortunate coincidence of primate lentiviral evolution? Nat Rev Microbiol *7*, 467-476.

Koppensteiner, H., Hohne, K., Gondim, M.V., Gobert, F.X., Widder, M., Gundlach, S., Heigele, A., Kirchhoff, F., Winkler, M., Benaroch, P.*, et al.* (2014). Lentiviral Nef suppresses iron uptake in a strain specific manner through inhibition of Transferrin endocytosis. Retrovirology *11*, 1.

Mackenzie, B., and Erickson, J.D. (2004). Sodium-coupled neutral amino acid (System N/A) transporters of the SLC38 gene family. Pflugers Arch *447*, 784-795.

Maldarelli, F., Chen, M.Y., Willey, R.L., and Strebel, K. (1993). Human immunodeficiency virus type 1 Vpu protein is an oligomeric type I integral membrane protein. J Virol *67*, 5056-5061.

Matheson, N.J., Peden, A.A., and Lehner, P.J. (2014). Antibody-free magnetic cell sorting of genetically modified primary human CD4+ T cells by one-step streptavidin affinity purification. PLoS One *9*, e111437.

Michel, N., Ganter, K., Venzke, S., Bitzegeio, J., Fackler, O.T., and Keppler, O.T. (2006). The Nef protein of human immunodeficiency virus is a broad-spectrum modulator of chemokine receptor cell surface levels that acts independently of classical motifs for receptor endocytosis and Galphai signaling. Mol Biol Cell *17*, 3578-3590.

Pickering, S., Hue, S., Kim, E.Y., Reddy, S., Wolinsky, S.M., and Neil, S.J. (2014). Preservation of tetherin and CD4 counter-activities in circulating Vpu alleles despite extensive sequence variation within HIV-1 infected individuals. PLoS Pathog *10*, e1003895.

Pozueta-Romero, J., Frehner, M., and Akazawa, T. (1991). Filtering centrifugation through two layers of silicone oil: a method for the kinetic analysis of rapid metabolite transport in organelles. Cell Struct Funct *16*, 357-363.

Qin, X.F., An, D.S., Chen, I.S., and Baltimore, D. (2003). Inhibiting HIV-1 infection in human T cells by lentiviral-mediated delivery of small interfering RNA against CCR5. Proc Natl Acad Sci U S A *100*, 183-188.

Ramirez, P.W., Famiglietti, M., Sowrirajan, B., DePaula-Silva, A.B., Rodesch, C., Barker, E., Bosque, A., and Planelles, V. (2014). Downmodulation of CCR7 by HIV-1 Vpu results in impaired migration and chemotactic signaling within CD4(+) T cells. Cell Rep *7*, 2019-2030.

Randow, F. (2006). Retroviral Transduction of DT40. In Reviews and Protocols in DT40 Research: Subcellular Biochemistry, J.-M. Buerstedde, ed. (Springer), pp. 383-386.

Rebhan, M., Chalifa-Caspi, V., Prilusky, J., and Lancet, D. (1997). GeneCards: integrating information about genes, proteins and diseases. Trends Genet *13*, 163.

Sauter, D., Schindler, M., Specht, A., Landford, W.N., Munch, J., Kim, K.A., Votteler, J., Schubert, U., Bibollet-Ruche, F., Keele, B.F.*, et al.* (2009). Tetherin-driven adaptation of Vpu and Nef function and the evolution of pandemic and nonpandemic HIV-1 strains. Cell Host Microbe *6*, 409-421.

Schaller, T., Ocwieja, K.E., Rasaiyaah, J., Price, A.J., Brady, T.L., Roth, S.L., Hue, S., Fletcher, A.J., Lee, K., KewalRamani, V.N.*, et al.* (2011). HIV-1 capsid-cyclophilin interactions determine nuclear import pathway, integration targeting and replication efficiency. PLoS Pathog *7*, e1002439.

Schmokel, J., Sauter, D., Schindler, M., Leendertz, F.H., Bailes, E., Dazza, M.C., Saragosti, S., Bibollet-Ruche, F., Peeters, M., Hahn, B.H.*, et al.* (2011). The presence of a vpu gene and the lack of Nef-mediated downmodulation of T cell receptor-CD3 are not always linked in primate lentiviruses. J Virol *85*, 742-752.

Sharp, P.M., and Hahn, B.H. (2010). The evolution of HIV-1 and the origin of AIDS. Philos Trans R Soc Lond B Biol Sci *365*, 2487-2494.

Takehisa, J., Kraus, M.H., Ayouba, A., Bailes, E., Van Heuverswyn, F., Decker, J.M., Li, Y., Rudicell, R.S., Learn, G.H., Neel, C.*, et al.* (2009). Origin and biology of simian immunodeficiency virus in wild-living western gorillas. J Virol *83*, 1635-1648.

Townsend, M.K., Clish, C.B., Kraft, P., Wu, C., Souza, A.L., Deik, A.A., Tworoger, S.S., and Wolpin, B.M. (2013). Reproducibility of metabolomic profiles among men and women in 2 large cohort studies. Clin Chem *59*, 1657-1667.

Tsitsiou, E., Sibley, C.P., D'Souza, S.W., Catanescu, O., Jacobsen, D.W., and Glazier, J.D. (2009). Homocysteine transport by systems L, A and y+L across the microvillous plasma membrane of human placenta. J Physiol *587*, 4001-4013.

Twentyman, P.R., and Luscombe, M. (1987). A study of some variables in a tetrazolium dye (MTT) based assay for cell growth and chemosensitivity. Br J Cancer *56*, 279-285.

van den Boomen, D.J., Timms, R.T., Grice, G.L., Stagg, H.R., Skodt, K., Dougan, G., Nathan, J.A., and Lehner, P.J. (2014). TMEM129 is a Derlin-1 associated ERAD E3 ligase

essential for virus-induced degradation of MHC-I. Proc Natl Acad Sci U S A *111*, 11425-11430.

Vigan, R., and Neil, S.J. (2010). Determinants of tetherin antagonism in the transmembrane domain of the human immunodeficiency virus type 1 Vpu protein. J Virol *84*, 12958-12970.

Vizcaino, J.A., Cote, R.G., Csordas, A., Dianes, J.A., Fabregat, A., Foster, J.M., Griss, J., Alpi, E., Birim, M., Contell, J.*, et al.* (2013). The PRoteomics IDEntifications (PRIDE) database and associated tools: status in 2013. Nucleic Acids Res *41*, D1063-1069.

Vizcaino, J.A., Deutsch, E.W., Wang, R., Csordas, A., Reisinger, F., Rios, D., Dianes, J.A., Sun, Z., Farrah, T., Bandeira, N.*, et al.* (2014). ProteomeXchange provides globally coordinated proteomics data submission and dissemination. Nat Biotechnol *32*, 223-226.

Weekes, M.P., Antrobus, R., Lill, J.R., Duncan, L.M., Hor, S., and Lehner, P.J. (2010). Comparative analysis of techniques to purify plasma membrane proteins. J Biomol Tech *21*, 108-115.

Weekes, M.P., Antrobus, R., Talbot, S., Hor, S., Simecek, N., Smith, D.L., Bloor, S., Randow, F., and Lehner, P.J. (2012). Proteomic plasma membrane profiling reveals an essential role for gp96 in the cell surface expression of LDLR family members, including the LDL receptor and LRP6. J Proteome Res *11*, 1475-1484.

Weekes, M.P., Tan, S.Y., Poole, E., Talbot, S., Antrobus, R., Smith, D.L., Montag, C., Gygi, S.P., Sinclair, J.H., and Lehner, P.J. (2013). Latency-associated degradation of the MRP1 drug transporter during latent human cytomegalovirus infection. Science *340*, 199-202.

Weekes, M.P., Tomasec, P., Huttlin, E.L., Fielding, C.A., Nusinow, D., Stanton, R.J., Wang, E.C., Aicheler, R., Murrell, I., Wilkinson, G.W.*, et al.* (2014). Quantitative temporal viromics: an approach to investigate host-pathogen interaction. Cell *157*, 1460-1472.

Werkheiser, W.C., and Bartley, W. (1957). The study of steady-state concentrations of internal solutes of mitochondria by rapid centrifugal transfer to a fixation medium. Biochem J *66*, 79-91.

Xia, J., Mandal, R., Sinelnikov, I.V., Broadhurst, D., and Wishart, D.S. (2012). MetaboAnalyst 2.0--a comprehensive server for metabolomic data analysis. Nucleic Acids Res *40*, W127-133.

Xia, J., Psychogios, N., Young, N., and Wishart, D.S. (2009). MetaboAnalyst: a web server for metabolomic data analysis and interpretation. Nucleic Acids Res *37*, W652-660.

Xia, J., Sinelnikov, I.V., Han, B., and Wishart, D.S. (2015). MetaboAnalyst 3.0-making metabolomics more meaningful. Nucleic Acids Res.

Zhang, H., Zhou, Y., Alcock, C., Kiefer, T., Monie, D., Siliciano, J., Li, Q., Pham, P., Cofrancesco, J., Persaud, D.*, et al.* (2004). Novel single-cell-level phenotypic assay for residual drug susceptibility and reduced replication capacity of drug-resistant human immunodeficiency virus type 1. J Virol *78*, 1718-1729.

Zheng, L., Baumann, U., and Reymond, J.L. (2004). An efficient one-step site-directed and site-saturation mutagenesis protocol. Nucleic Acids Res *32*, e115.